CONFINEMENT MODEL FOR CONCRETE COLUMNS INTERNALLY REINFORCED WITH GLASS FIBER REINFORCED POLYMER SPIRALS

by

Priyank Pravin Sankholkar

A thesis submitted to the faculty of
The University of Utah
in partial fulfillment of the requirements for the degree of

Master of Science

Department of Civil and Environmental Engineering

The University of Utah

August 2016

The University of Utah Graduate School

STATEMENT OF THESIS APPROVAL

The thesis of **Priyank Pravin Sankholkar**

has been approved by the following supervisory committee members:

Christopher P. Pantelides	, Chair	**May 03, 2016** Date Approved
Luis F. Ibarra	, Member	**April 29, 2016** Date Approved
Amanda C. Bordelon	, Member	**April 29, 2016** Date Approved

and by **Michael E. Barber**, Chair/Dean of

the Department/College/School of **Civil and Environmental Engineering**

and by David B. Kieda, Dean of The Graduate School.

ABSTRACT

This research investigates confinement of concrete using glass fiber reinforced polymer (GFRP) spirals. Concrete prisms 10 in. in diameter and 30 in. high were internally reinforced with GFRP spirals. Using different configurations of GFRP spirals, 21 prisms were built; in addition, three prisms were built without any reinforcement. The different series of specimens with GFRP spirals were created by varying the bar diameter and pitch. The bar sizes used for spirals were #3, #4 and #5. The pitch used for #3 spirals was 1.5 in., 2 in. and 3 in. The pitch used for #4 spirals was 1.5 in. and 2 in. The pitch used for #5 spirals was 1.5 in., 2 in. and 2.5 in. Wooden dowels were used to hold the spirals at the required pitch. Compression tests were conducted for each specimen and results were obtained in the form of axial load, axial stress, axial strain and hoop strain. A concrete confinement model was obtained which describes the increase in both compressive strength and axial strain of concrete confined internally with GFRP spirals. The confinement model was verified with tests conducted on four concrete columns reinforced with GFRP spirals and GFRP longitudinal bars and similar specimens from the literature. The four columns were 8 in. in diameter and 30 in. high reinforced with #3 GFRP spirals at a pitch of 1.5 in. and had either four or six #5 longitudinal GFRP bars. The agreement between the model and the columns was satisfactory for both confined concrete strength and ultimate axial compressive strain.

TABLE OF CONTENTS

LIST OF TABLES

LIST OF FIGURES

ACKNOWLEDGEMENTS

I would like to express my appreciation to my mentor and advisor Dr. Chris Pantelides for his support, guidance and encouragement. I would also like to thank my committee members Dr. Luis Ibarra and Dr. Amanda Bordelon for their advice and assistance not only during the research but throughout my time at University of Utah.

I would like to give special thanks to Mark Bryant, the lab manager, for his constant support and help during my research. Also I would like to thank many individuals for helping me during building, casting and testing of the specimens. These individuals include, Ruoyang Wu, Joel Parks, Trevor Nye, M. J. Ameli, Thomas Hales and Ryan Barton.

I would also like to thank my parents Pravin Sankholkar and Anagha Sankholkar for supporting me throughout my educational career.

CHAPTER 1

INTRODUCTION AND LITERATURE REVIEW

The concept of strengthening structures with fiber reinforced polymer (FRP) composites has been used for many years. FRP composites have been successfully used in the aerospace and automobile industries for a long time. In the construction industries, FRP composites have been used for strengthening existing structures; for example, FRP wraps or FRP jackets are bonded on the surface of concrete structures for the purpose of retrofit or rehabilitation. There are a number of situations where the load-carrying capacity of a structure in service may need to be increased. In such cases, using FRP wraps would be easier and more economical than the old technique of bonding steel plates to the surface of the tension zone with adhesives and bolts. FRP composites have many advantages over steel plates: for instance, they can be formed in place into complicated shapes, and they can also be easily cut to the desired length and size on site. FRP composites are lighter than steel plates and have equivalent or higher strength in tension. The installation of FRP composites is much simpler and eliminates the requirement of any kind of temporary supports and heavy lifting equipment.

Recently, FRP composites have become common materials for strengthening concrete bridges. Strength degradation is observed in concrete bridges after a period of 20-30 years; in this case, rehabilitation of certain structural members of the bridge is required. FRP composites wraps and jackets can be used to strengthen the structural elements of the

bridge. This approach is considered to be more economical and less disruptive than replacement. Generally, steel spirals are used in the concrete columns of bridges for confining the concrete. In bridges built over water-bodies or in areas where salt is used for snow removal, corrosion is an important factor of consideration. However, cracks in the concrete structure initiate corrosion of even the epoxy coated steel bars. In such cases, FRP composite bars and spirals can be used as an alternative to steel reinforcement.

FRP reinforcement has a different mechanical behavior than steel reinforcement. The major difference is that FRP reinforcement does not yield and shows elastic behavior until failure. Steel reinforcement is ductile in nature, whereas FRP reinforcement possess brittle characteristics. This is an important factor when FRP bars are considered for new construction. Glass fiber reinforced polymer (GFRP) composites have a lower modulus of elasticity as compared to reinforcing steel. This lower modulus of elasticity needs to be taken into consideration for finding the deflection of structural elements. The tensile strength of GFRP is also higher than steel, which increases the tensile capacity of the structural element.

Previous research for structures with internal FRP reinforcement has focused on the following categories: (1) analysis of short and slender concrete columns with internal FRP reinforcement, (2) analysis of concrete columns subjected to corrosion with internal FRP reinforcement, and (3) development of a stress-strain model for confined concrete with FRP spirals.

Research has been conducted on concrete confined externally with FRP jackets, FRP composite spirals or FRP hoops. Mander et al. (1988) developed a stress-strain model for concrete subjected to uniaxial compressive loading and confined by transverse steel

reinforcement with either spirals, circular or rectangular hoops; they concluded that reinforced concrete members with axial compressive forces may be confined using transverse steel to enhance the member strength and ductility. Mander et al. (1988) found that the form of the stress-strain curve for confined concrete can be expressed in terms of a simple uniaxial relation which only requires three parameters: (1) compressive strength of confined concrete, (2) ultimate axial compressive strain of confined concrete and (3) modulus of elasticity of concrete.

Lam and Teng (2003) developed a simplified stress-strain model for concrete confined with external FRP reinforcement (FRP wraps); the FRP wraps were predominantly oriented in the hoop direction. Lam and Teng (2003) determined that the average hoop strain of the FRP wraps at rupture was lower than the ultimate tensile strain of the FRP laminate. This indicated that the assumption of FRP rupture when the material tensile strength is reached was not valid. The reason for this is the effect of axial stress and hoop stress interaction as well as the effect of the geometry of the bent fibers. Lam and Teng (2003) also proposed a new design-oriented stress-strain model suitable for direct use in design. The model accounted for the stiffness of FRP jackets and the ultimate tensile capacity of the FRP jacket.

Moran and Pantelides (2012) developed a stress-strain model that describes the compressive and dilation performance of elliptical and circular FRP-confined sections; they used the concepts of diagonal dilation and equilibrium of FRP-confined concrete. The analysis of the dilation behavior of circular and elliptical FRP-confined concrete sections shows that at very low jacket stiffness, the jacket is not effective in providing adequate lateral restraint against unstable crack growth. The effectiveness of the FRP jacket

curtailing this unstable crack growth increases with increasing stiffness of the FRP jacket.

Alsayed et al. (1999) performed compressive tests on concrete columns having a rectangular cross-section and reinforced with internal FRP bars. The tests were conducted on fifteen specimens having a cross-section of 10 in. by 18 in. and height of 47 in. Each specimen consisted of six 0.62 in. diameter longitudinal steel or GFRP bars and nine 0.24 in. diameter transverse steel or GFRP ties. It was found that replacing the longitudinal steel bars with GFRP bars of equivalent size reduces the axial capacity of the columns by an average of 13%. The experimental results also showed that replacing steel ties with GFRP ties, while keeping the same reinforcement ratio, reduces the axial capacity by approximately 10%; the material type of ties, i.e., steel versus GFRP, has a great influence on the ascending part of the load versus axial shortening curve of the column.

Mirmiran et al. (2001) performed a study to determine if the use of FRP internal bars makes reinforced concrete more susceptible to slenderness effects due to the lower stiffness and compression contribution of FRP reinforcing bars. This was observed in columns with a minimum longitudinal reinforcement ratio of 1% and where steel reinforcement was replaced with an equivalent amount of FRP reinforcement. It was found that for rectangular concrete columns reinforced with internal longitudinal FRP bars, the interaction diagram does not exhibit a balanced point as defined by the ACI building code (ACI 318, 2014) due to yielding of the steel reinforcement as opposed to linear elastic behavior of the FRP bars.

De Luca et al. (2010) studied the behavior of full-scale GFRP reinforced concrete columns under axial load. The square columns had a cross-section of 2 ft x 2 ft and a height of 10 ft and were tested under axial load. The results for columns reinforced with lateral GFRP ties were compared with tests performed on steel reinforced columns with an

identical reinforcement configuration. All columns were reinforced with eight #8 longitudinal bars with their respective material type and #4 ties as lateral reinforcement. The spacing of lateral GFRP ties was 3 in. or 12 in. and the spacing for steel ties was 16 in. to account for the lower modulus of elasticity of the GFRP material. They determined that the GFRP reinforcement contributes very little to the axial load capacity of the column and that a tie spacing of 3 in. provided a more desirable level of ductility than the tie spacing of 12 in.

Additional axial load tests were performed on square columns reinforced with GFRP vertical bars and GFRP lateral ties by Tobbi et al. (2012). The columns had a cross-section of 14 in. x 14 in. and a height of 55 in. The columns were tested using four different tie configurations, using 0.5 in. diameter bar with spacing of either of 4.72 in. or 3.15 in. Three tie configurations utilized eight 0.75 in. diameter longitudinal bars and one tie configuration utilized twelve 0.63 in. diameter longitudinal bars. They concluded that the use of GFRP ties can be effective for providing confinement and also reported that reducing the tie spacing from 4.72 in. to 3.15 in. increases the strength by 20%. It was estimated that the compressive strength of the GFRP bars was approximately 35% of the maximum tensile strength.

Pantelides et al. (2013) explored the option of replacing steel spirals with GFRP spirals to reduce chloride induced corrosion of longitudinal steel bars in hybrid columns. They tested columns with internal GFRP spirals or steel spirals with longitudinal steel or GFRP reinforcement under axial compressive load to failure. Some of the specimens were subjected to accelerated corrosion and subsequently were tested under axial load to failure. The experimental results showed that hybrid columns and all-GFRP columns achieved

87% and 84%, respectively, of the axial load capacity of all-steel columns. Pantelides et al. (2013) concluded that to achieve similar performance to all-steel columns, hybrid columns must be reinforced with a larger GFRP spiral reinforcement ratio. All-GFRP columns should have a larger reinforcement ratio for both longitudinal bars and spirals. Most of the corrosion in the all-steel columns was observed in the spirals. This is a matter of concern since concrete looses its confinement and the column fails in a brittle manner.

Afifi et al. (2015) investigated the compressive behavior of circular concrete columns longitudinally reinforced with Carbon FRP (CFRP) bars and CFRP spirals. Their experiments suggest that GFRP spirals can effectively confine the concrete core. They also concluded that columns reinforced with GFRP spirals attained slightly higher strength than columns reinforced with GFRP rectangular hoops. A new confined concrete model was proposed for GFRP reinforced concrete columns to predict the maximum concrete core stress.

Hales (2015) evaluated the behavior of short and slender high-strength concrete columns reinforced with GFRP bars and spirals subjected to concentric and eccentric axial loads. The experimental results showed that slender columns with a double layer of longitudinal reinforcement consisting of inner steel and outer GFRP longitudinal bars with inner and outer GFRP spirals had a better overall performance compared to the slender columns with a single layer of reinforcement. It was observed that the failure mode for short and slender columns with low eccentricities was a material type of failure consisting of compressive failure of concrete, tensile rupture of GFRP spiral, compressive rupture of longitudinal GFRP bars or compressive buckling of longitudinal steel bars. The failure mode of short and slender columns with large eccentricities was a stability type, buckling

failure with concrete cover on the compressive side breaking away at mid-height. They also concluded that GFRP spirals and GFRP longitudinal bars are a viable method of reinforcement for short and slender concrete columns. However, due to their lower modulus of elasticity, GFRP spirals should be provided with a larger cross-sectional area and smaller pitch as compared to steel spirals to obtain similar confinement levels. GFRP longitudinal bars can provide larger deflection capacity compared to steel longitudinal bars since they have a larger tensile strength. In addition, they provide a self-centering effect after removal of the load, which is beneficial for transient type loads such as earthquakes.

Karim et al. (2016) developed a model for load-deformation of concrete columns reinforced with GFRP bars and helices. They also investigated the behavior of GFRP reinforced columns considering the helix pitch effect. Karim et al. (2016) used #4 GFRP bars as the longitudinal reinforcement and #3 GFRP helices as transverse reinforcement. They tested total of 5 circular columns under concentric axial loading. The general GFRP reinforced columns experienced two peak axial load. The first peak load represents maximum load carrying capacity of the gross concrete section, while the second peak load indicates the maximum load carrying capacity of concrete confined by GFRP helices. This study also concluded that longitudinal GFRP bars improved the first and second peak loads and confined concrete strength of GFRP reinforced columns.

In this study, confinement of concrete using GFRP spirals is evaluated. The aim of this research is to develop equations for the compressive strength (f'_{cc}) and the ultimate axial compressive strain (ε_{ccu}) of concrete confined by GFRP spirals. Equations are proposed for design of new concrete columns reinforced with GFRP longitudinal bars and spirals.

CHAPTER 2

EXPERIMENTAL PROGRAM

This chapter describes construction of the specimens used to achieve the objective of the experimental portion of the research. The specifications for the materials used, preparations for testing and testing methods are discussed in this chapter.

2.1 Objectives

The objectives of this research are as follows:

1. Investigate the performance of concrete prisms internally reinforced with GFRP spirals under axial compression. There are no longitudinal bars in the prisms; wooden dowels are used to maintain a fixed pitch for the GFRP spirals.
2. Investigate the variation in axial stress according to changes in bar diameter and the pitch of GFRP spirals.
3. Investigate the ultimate hoop strain of GFRP spirals.
4. Investigate the confining stresses for each type of specimen reinforced with GFRP spirals of different diameter and pitch.
5. Develop an equation for the compressive strength of confined concrete and ultimate axial compressive strain similar to the equations in ACI 440.2R-08, for columns reinforced with GFRP longitudinal bars and GFRP spiral.

6. Validate the model with axial compression tests of concrete columns reinforced with GFRP longitudinal bars and spirals.

2.2 Description and construction of specimens

Medium-scale concrete prisms of 10 in. diameter and 30 in. high were built for testing. These specimens were called prisms instead of columns since they did not have any longitudinal reinforcement inside the concrete. Instead of providing any longitudinal reinforcement, the GFRP spirals were held at the required pitch with the help of wooden dowels. A total of 24 prism specimens were built, out of which three were just plain concrete without any reinforcement. In addition, four column specimens were built. These four specimens had a diameter of 8 in., a height of 30 in. and were reinforced with either four or six #5 longitudinal GFRP bars. The GFRP spirals used for these specimens were #3 at pitch of 1.5 in. A typical elevation and the section of a prism and a column are shown in Figure 2.1 and Figure 2.2, respectively. Pea gravel was used as coarse aggregate in the concrete mix to cast the specimens. The design compressive strength of concrete was 4,000 psi and the slump was 6.75 in. The mix design for concrete is shown in Table 2.1. Thirty 4x8 cylinders were cast from the same concrete. The average compressive strength of the concrete cylinders at 28 days was 5,900 psi. Dry curing of the specimens was performed in the laboratory.

The prisms were divided into categories based on the bar diameter of the GFRP spirals and the pitch. The bar diameter sizes for the GFRP spirals were #3, #4 and #5. The pitch for #3 spirals was 1.5 in., 2 in. and 3 in. with three specimens for each pitch. The pitch for #4 spirals was 1.5 in. and 2 in. with three specimens for each pitch. The pitch for #5 spirals was 1.5 in., 2 in. with three specimens for each pitch. For the three specimens with a #5

spirals at 2 in. pitch, two specimens had a slightly larger pitch of 2.5 in. This was caused because the wooden dowels were unable to hold a #5 spiral at 2 in. This construction error was rectified by considering the value of the pitch as 2.5 in. in the evaluation and analysis of these two specimens. The specimens were numbered from 1 to 28, and were denoted by the size of spiral and its pitch. The specimen numbers and its type are listed in Table 2.2. For instance, specimen 1 was #3@1.5, where #3 denotes the bar diameter size and 1.5 is the pitch of the GFRP spiral in inches. The concrete columns were denoted as 4LR#3@1.5, where 4LR represents the number of longitudinal reinforcing bars. All the longitudinal reinforcing bars were #5 diameter GFRP bars. The variation in bar diameter size and the pitch of GFRP spirals for prisms and columns is shown in Figs. 2.3 and 2.4, respectively. The measurement of the cross-sectional area of the bars was performed using water immersion tests by the manufacturer, as required by ACI 440.3R-04. The properties of the GFRP spirals used are described in Table 2.3.

Sonotubes 10 in. diameter and 30 in. high were used for casting the prisms; sonotubes 8 in. diameter and 30 in. high were used for casting the concrete columns. The sonotubes were fixed at the bottom on wooden planks with steel brackets. Small pieces of wooden dowels were fixed on the outer surface of the GFRP spirals on the top and bottom of the specimen with glue. The pieces of wooden dowels helped in maintaining the clear cover of concrete to 0.5 in., as shown in Figure 2.5. The specimens were arranged on the wooden planks as shown in Figure 2.6.

2.3 Instrumentation and test preparation of specimens

The concrete prisms were instrumented to measure hoop and axial strain at the mid-height of the specimens. The hoop strain was measured with strain gauges attached to the

GFRP spirals, while the axial strain was measured using linear variable displacement transformers (LVDTs). The strain gauges were placed on the spirals at mid-height of the concrete prisms. As there were three specimens for each type, one had four strain gauges placed 90 degrees around the spiral, while the other two specimens had three strain gauges placed 120 degrees around the spiral. The strain gauges were located at a different height due to the spiral shape. The strain gauges were protected with a coating to avoid damage while casting as shown in Figure 2.7. This coating also protected the strain gauges from water in the concrete. The strain gauge wires were guided out from the top of the concrete prisms to the side. For specimens with longitudinal GFRP bars, three strain gauges 120 degrees apart were attached on the GFRP spiral and one strain gauge was attached on one of the longitudinal GFRP bars.

Two vertical LVDTs were used for each prism and were placed 180 degrees apart. The LVDTs were wrapped with foam to protect them from damage during the test, as shown in Figure 2.8. These LVDTs were placed on steel brackets which were attached to the concrete prisms using epoxy. The strain gauges and LVDTs were calibrated before the start of each test using StrainSmart 7000 Version 4.7, a program made by VISHAY Micro-measurements, which was the data acquisition system used. The number of strain gauges and the gauge length of LVDTs for each specimen is listed in Table 2.2. For number of strain gauges in Table 2.2, RD represents hoop direction while LD represents longitudinal direction.

Since the strain gauges were attached at the prism's mid-height, there was a need to avoid failure at the top and bottom of the prisms. To avoid premature end crushing, the prisms were wrapped with one layer of Carbon Fiber Reinforced Polymer (CFRP) on the top and bottom as shown in Figure 2.9; the width of each layer was 8 in. The CFRP wraps

were bonded to the concrete surface using epoxy resin. After wrapping, the CFRP wraps were allowed to cure for seven days to attain full strength. Steel collars, 6 in. long and 0.5 in. thick, were used to confine the top and bottom of the prisms. The collars were built in two halves and were tightened around the prism with four bolts having a diameter of 0.5 in. Care was taken not to damage any of the strain gauge wires coming out of the top.

The specimens were tested under controlled monotonic axial compressive load which was applied with the help of a W14X342 steel column. The steel column was attached to a hydraulic actuator. A loading rate of 0.05 in. per minute was selected for these tests. This rate was slow enough to avoid dynamic effects for the test results. The displacement of the actuator was controlled by a temposonic LVDT. High density polyethylene sheet (HDPE) was used to distribute the load on the concrete prisms, as shown in Figure 2.10. To obtain the confined strength of the prisms, only the area inside the spirals was loaded. The diameter of the HDPE plate was 8.5 inches for the prisms and 6.5 inches for the columns with vertical GFRP bars. The thickness of the HDPE plate was 0.5 in. These plates were placed at both the top and bottom of the prism. To reduce possible eccentricities in loading, the specimens were placed on a swivel base steel plate, as shown in Figure 2.11. The general experimental setup for the specimens is shown in Figure 2.12.

Table 2.1: Mix design for concrete.

Material	Required	Batched
Cement Type-B	908 lb	905 lb
Fly ash	150 lb	140 lb
Pea gravel	1256 lb	1240 lb
Sand	3053 lb	3040 lb
Water	43.9 gl	43.7 gl
Reducer	23 oz	22 oz
Super	126 oz	120 oz

Table 2.2: Specimen number and its type with number of strain gauges used and gauge length for the LVDTs.

Specimen Number	Type of specimen	Number of strain gauges and its position	Gauge length for both the LVDTs (in.)
1	#3@1.5	4 RD, 0 LD	10
2		3 RD, 0 LD	10
3		3 RD, 0 LD	10
4	#3@2	4 RD, 0 LD	10
5		3 RD, 0 LD	10
6		3 RD, 0 LD	10
7	#3@3	4 RD, 0 LD	10
8		3 RD, 0 LD	10
9		3 RD, 0 LD	10
10	#4@1.5	4 RD, 0 LD	10
11		3 RD, 0 LD	10
12		3 RD, 0 LD	10
13	#4@2	4 RD, 0 LD	10
14		3 RD, 0 LD	10
15		3 RD, 0 LD	10
16	#5@1.5	4 RD, 0 LD	19.5
17		3 RD, 0 LD	19.5
18		3 RD, 0 LD	19.5
19	#5@2	4 RD, 0 LD	10
20	#5@2.5	3 RD, 0 LD	10
21		3 RD, 0 LD	10
22	Plain concrete without any reinforcement	0 RD, 0 LD	10
23		0 RD, 0 LD	10
24		0 RD, 0 LD	10
25	4LR#3@1.5	3 RD, 1 LD	19.5
26		3 RD, 1 LD	19.5
27	6LR#3@1.5	3 RD, 1 LD	19.5
28		3 RD, 1 LD	19.5

Table 2.3: Properties of GFRP spirals.

Size of bar	Nominal diameter (in.)	Nominal area ($in.^2$)	Tensile modulus of elasticity (psi x 10^6)	Ultimate Strain (%)
#3	3/8	0.1324	6.7	1.79
#4	1/2	0.2273	6.7	1.64
#5	5/8	0.3287	6.7	1.57

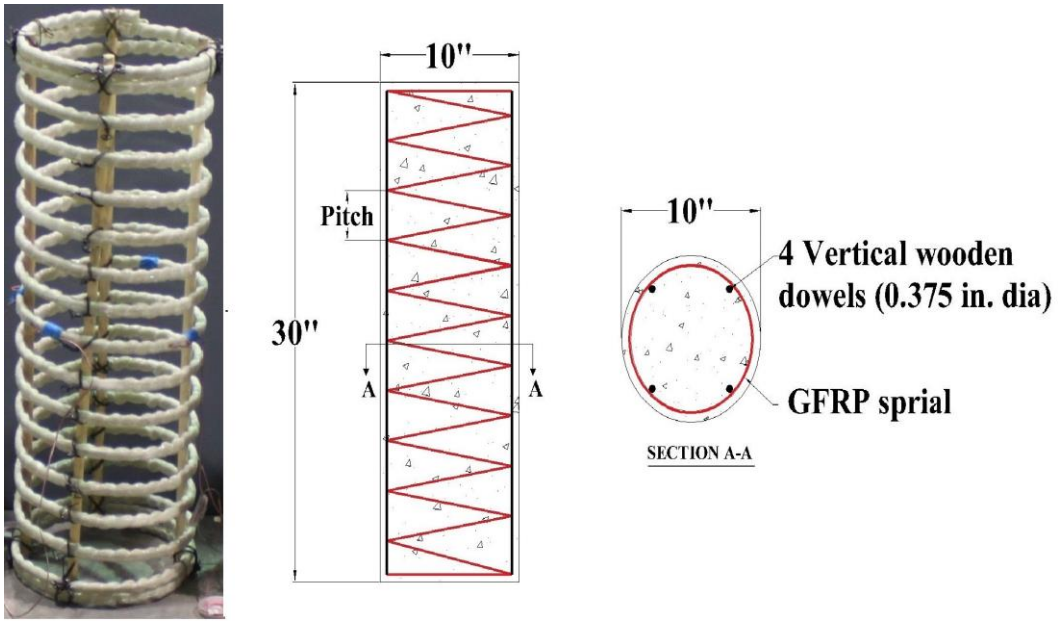

Figure 2.1: GFRP reinforced concrete prisms.

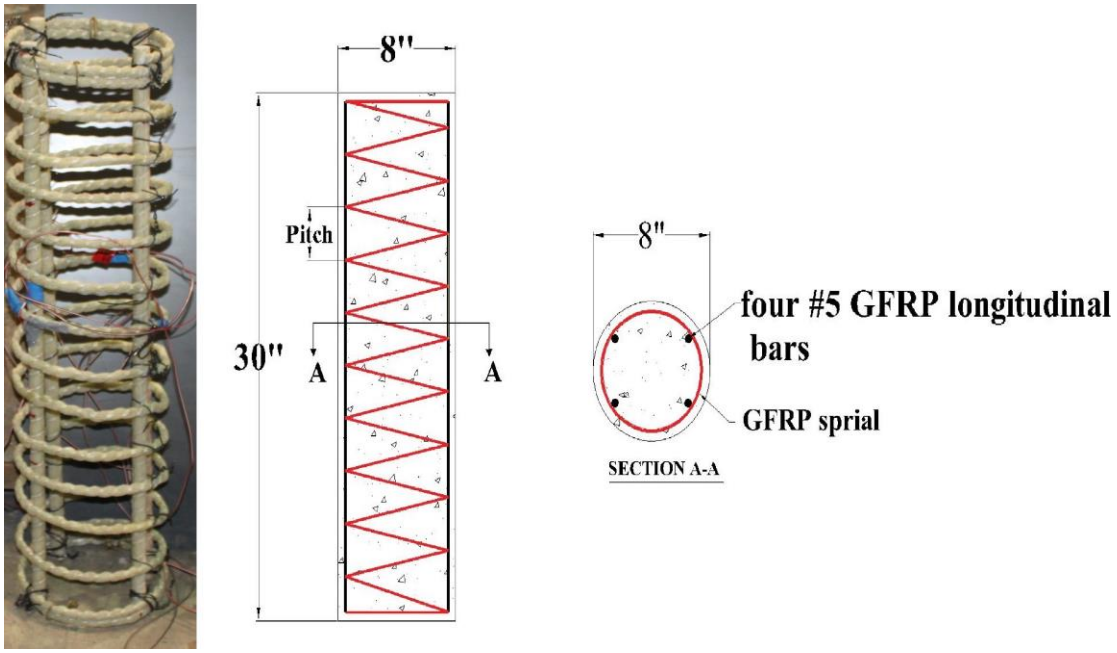

Figure 2.2: GFRP reinforced concrete columns.

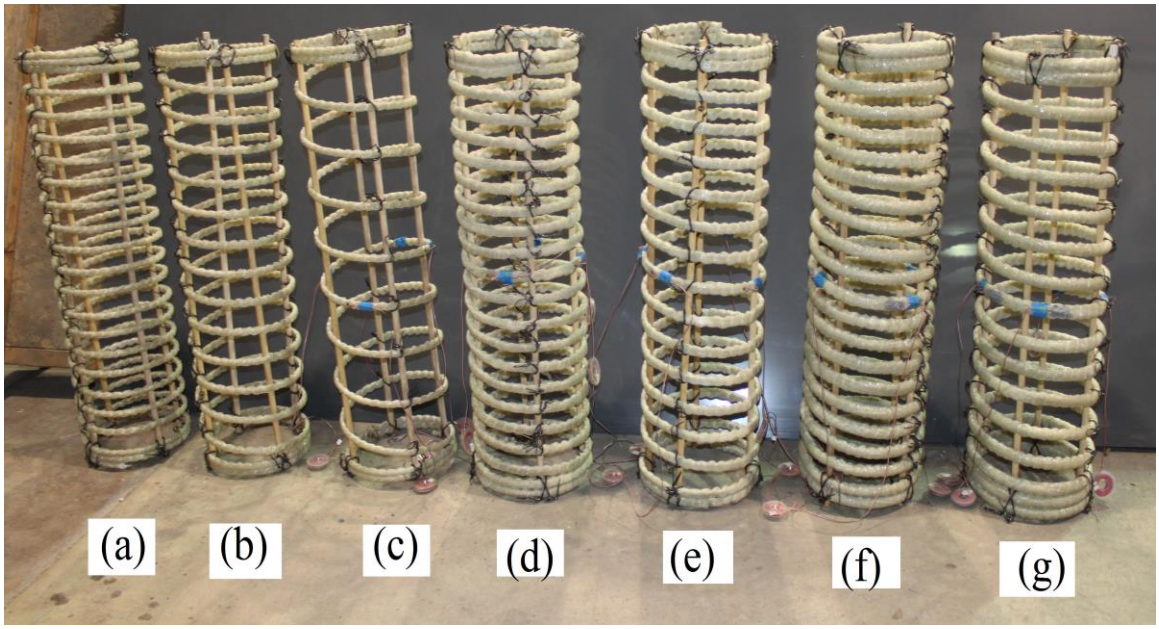

Figure 2.3: Variation in bar sizes and pitches of the prisms (a) #3@1.5; (b) #3@2; (c) #3@3; (d) #4@1.5; (e) #4@2; (f) #5@1.5; (g) #5@2.

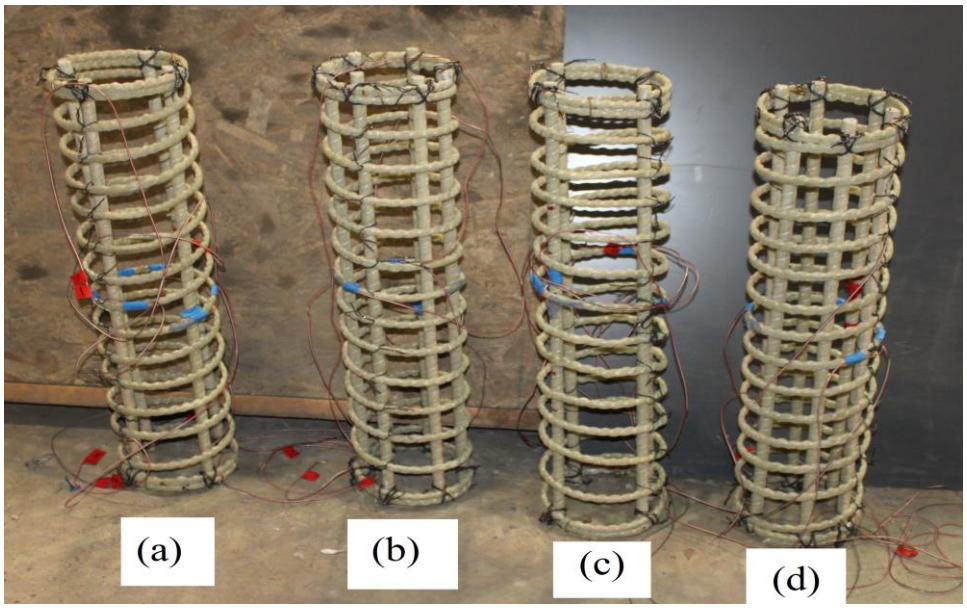

Figure 2.4: GFRP cages for the columns (a) 4LR#3@1.5; (b) 6LR#3@1.5; (c) 4LR#3@1.5; (d) 6LR#3@1.5.

Figure 2.5: Wooden dowels used to maintain clear cover of concrete and pitch of the spiral.

Figure 2.6: GFRP cages placed in sonotubes and fixed on wooden planks with steel brackets.

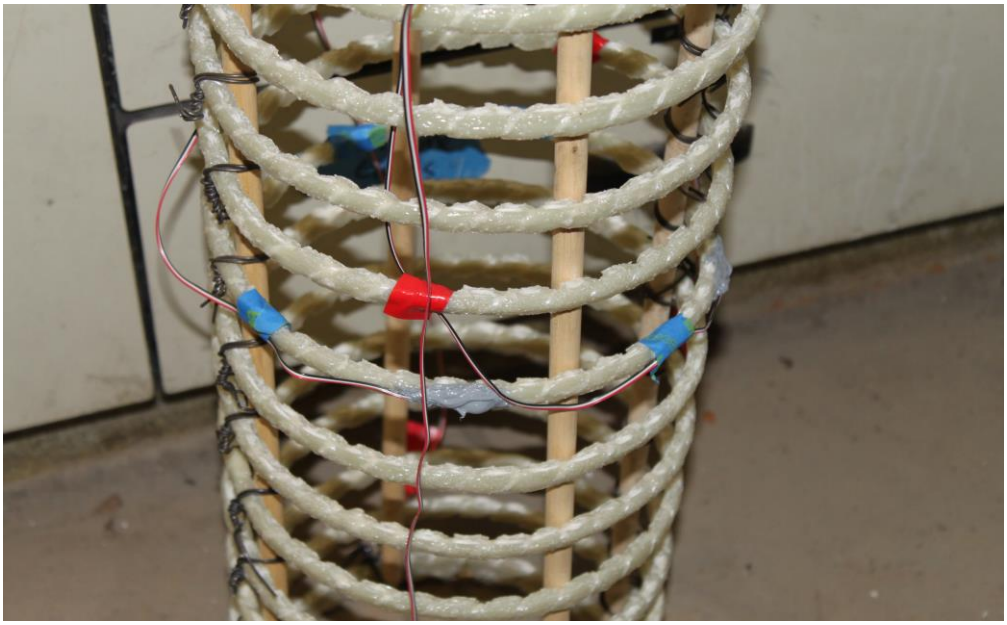

Figure 2.7: Internal strain gauge with protective coating.

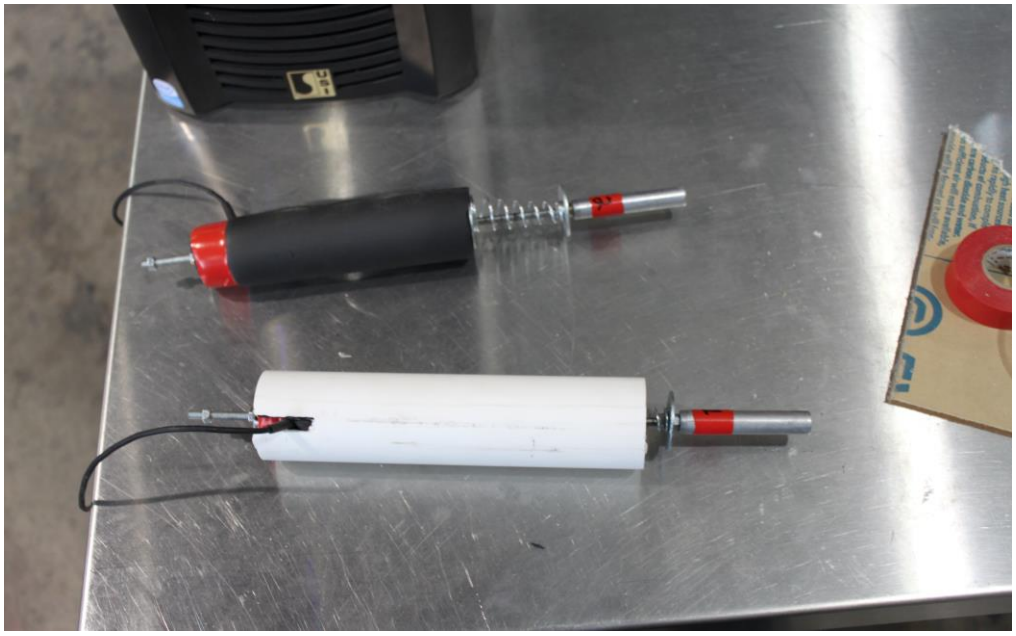

Figure 2.8: Protective covering for LVDTs.

Figure 2.9: CFRP wraps on the top and bottom of specimens.

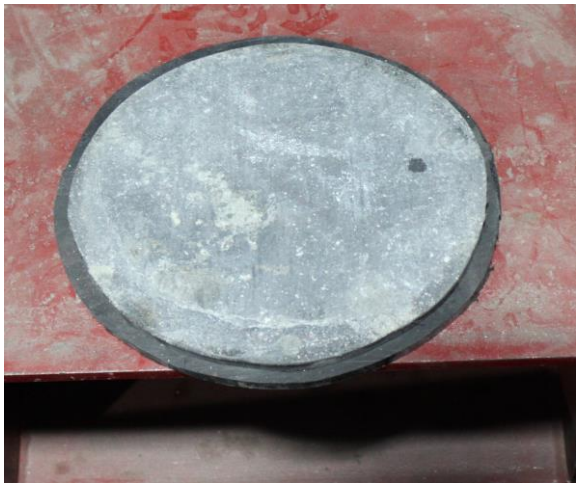

Figure 2.10: HDPE plates used to distribute the load.

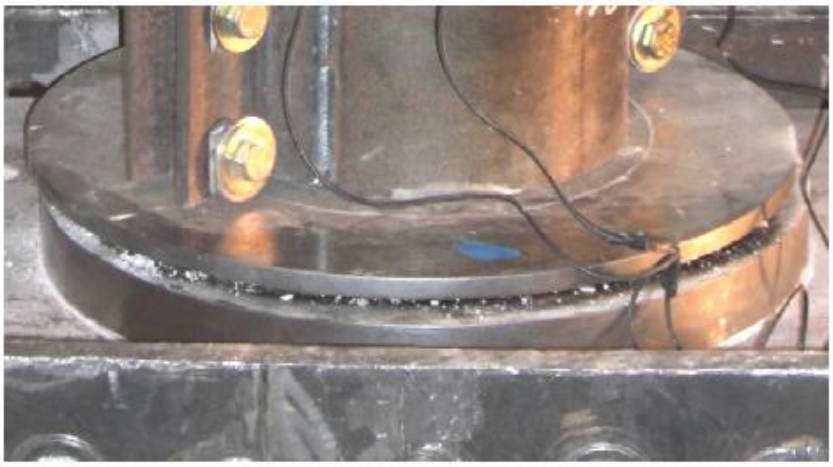

Figure 2.11: Swivel base plate.

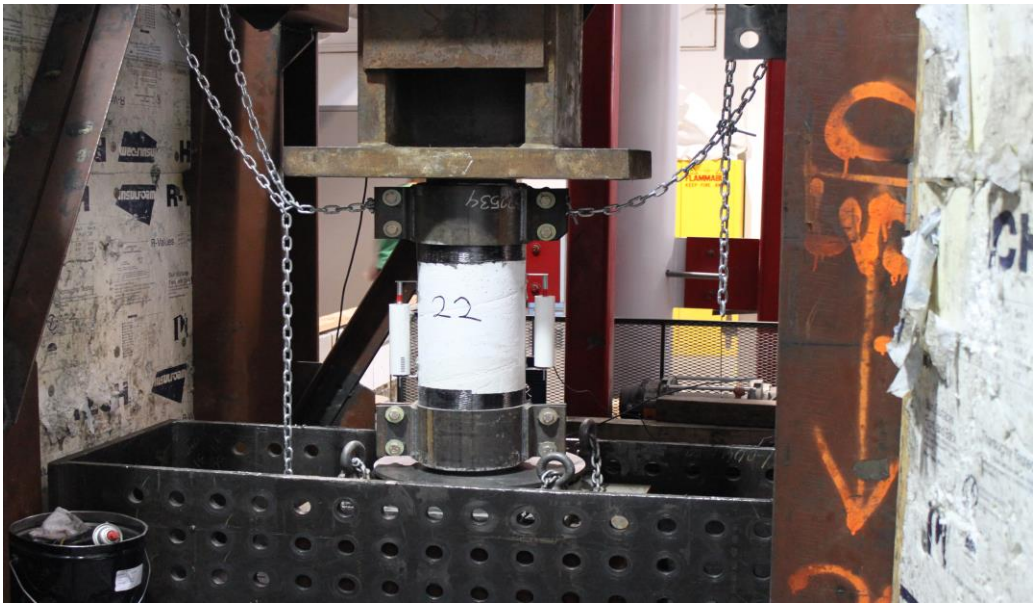

Figure 2.12: Setup for test with steel collars and position of two LVDTs.

CHAPTER 3

EXPERIMENTAL RESULTS

This chapter explains the results obtained from the compression tests concrete prisms and columns. The chapter includes a discussion on how variation of the diameter and pitch of the spiral affects concrete confining stress.

The most common method of evaluating the performance of columns under axial compression is the stress versus strain curve. The stress values were calculated by dividing the value of the applied load obtained from the load cell by the column effective cross-sectional area. The effective area loaded for the concrete prisms was 56.74 $in.^2$ and the area loaded for the concrete columns was 33.18 $in.^2$. The axial strain was obtained by dividing the displacement of the LVDT by its gauge length. The gauge length for the concrete prisms except the three #5@1.5 prisms and the four concrete column was 10 in. The gauge length for the three #5@1.5 prisms and the four concrete columns was 19.5 in. The hoop strain was obtained directly from strain gauges attached to the GFRP spirals.

Due to the confinement provided by the steel collars and CFRP wraps for a length of 8 in. top and bottom, failure occurred in the desired region, i.e., the mid-height of the prism or column. Three 4x8in. concrete cylinders were tested on the test day with an average compressive strength ($f`_{co}$) of 7,200 psi.

3.1 Results from compression tests of concrete prisms

It was observed that higher axial load values were achieved by specimens with a larger spiral cross-sectional area and a smaller spiral pitch. This shows that higher confinement stresses were achieved using GFRP spirals with a larger cross-sectional area. The load at which the GFRP spiral ruptured was considered as the load at failure, after which the test was terminated. The maximum load that was observed was 692 kips for a specimen with #5 spirals and pitch of 1.5 in. The lowest load at which a specimen failed was 332 kips, for a specimen with #3 spirals and 3 in. pitch. Table 3.1 lists the axial compression load at failure and confinement stress for the concrete prisms. The failure observed for the concrete prisms was a material type failure consisting of compressive failure of the concrete and tensile rupture of the GFRP spirals. It was expected that the prisms, internally reinforced with GFRP spirals, would show a brittle type of failure. Also for a particular diameter of the GFRP spiral bar, the damage caused to the GFRP spirals was higher in the case of a smaller pitch. For #3@1.5, an average of four spirals ruptured, similarly for #3@2 and #3@3, an average of three and one spirals ruptured, respectively. For specimens with #4 spirals, an average of four GFRP spirals ruptured at failure. For #5@1.5, an average of three GFRP spirals ruptured, while for #5@2, an average of two spirals ruptured.

Higher values of hoop strain were observed for spirals of greater cross-sectional area and smaller pitch. The hoop strain obtained from strain gauges attached to GFRP spirals did not exceed the ultimate tensile strain provided by the manufactures. The highest value of 0.01453 in./in. of hoop strain was achieved for specimen 16 which was type #5@1.5. Axial strains measured with LVDTs followed the same pattern of variation as hoop strain. The maximum hoop and axial strains for each specimen are shown in Table 3.1. The

average axial strain obtained from the LVDTs for the concrete prisms without any reinforcement was 0.00189 in./in. and the standard deviation was 0.0003 in./in. This axial strain is close to the maximum strain of unconfined concrete (ε'_c) of 0.002 in./in. as given in ACI 440.2R-08. The concrete prisms after failure are shown in Figure 3.1 to Figure 3.9.

3.2 Results from compressive load tests of concrete columns

The concrete columns had a diameter of 8 in. with an area of 33.18 in.^{2} loaded under a compressive axial load. From the tests, it was observed that higher confinement stress was achieved for columns with six longitudinal bars than for columns with four longitudinal bars. Thus, the results show that the amount of longitudinal reinforcement provided in the column contributes to the confinement of the concrete core. The highest load of 366 kips was achieved for column 6LR#3@1.5. A maximum ultimate hoop and axial strain of 0.0208 in./in. and 0.0138 in./in., respectively, was achieved for column 6LR3#@1.5. Similarly, a maximum ultimate hoop and axial strain of 0.00694 in./in. and 0.00661 in./in. was achieved for specimen 4LR#3@1.5. The failure load, confined stress, maximum hoop strain and maximum axial strain for each column are described in Table 3.2. The concrete columns reinforced with GFRP spirals and longitudinal bars showed a brittle type of failure. On average, GFRP spirals ruptured at three places; longitudinal bars ruptured for 4LR#3@1.5 type of specimens. The all-GFRP reinforced concrete columns after failure are shown in Figures 3.10-3.12.

Table 3.1: Experimental data for concrete prisms.

Specimen No.	Specimen type	Load at failure (kips)	Experimental confined stress (ksi) (f'_{cc})	Maximum hoop strain (in./in.)	Maximum axial strain (in./in.)
1	#3@1.5	452.87	7.98	0.0108	0.0093
2		491.68	8.66	0.0139	0.0135
3		508.78	8.96	0.0124	0.0042
4	#3@2	400.6	7.05	0.0106	0.0107
5		421.36	7.42	0.0079	0.0064
6		402.37	7.09	0.0092	0.0043
7	#3@3	332.1	5.85	0.0097	0.0087
8		390.68	6.88	0.0087	0.0037
9		336.17	5.92	0.0091	0.0092
10	#4@1.5	500.94	8.82	0.0093	0.0121
11		532.67	9.38	0.015	0.0121
12		523.38	9.22	0.0102	0.0121
13	#4@2	450.21	7.93	0.0091	0.0094
14		468.41	8.25	0.0099	0.0057
15		451.48	7.95	0.0092	0.0057
16	#5@1.5	691.89	12.19	0.0145	0.0148
17		657.69	11.59	0.0128	0.0148
18		628.12	11.06	0.0066	0.0094
19	#5@2	584.09	10.29	0.0117	0.0078
20	#5@2.5	477.3	8.41	0.0054	0.0054
21		477.58	8.41	0.0039	0.0028
22	Plain Concrete	412.37	5.25	-	0.0017
23		446.08	5.67	-	0.0023
24		372.26	4.73	-	0.0015

Table 3.2: Experimental data for GFRP reinforced concrete columns

Specimen No.	Specimen type	Load at failure (kips)	Experimental confined stress (ksi)	Maximum hoop strain (in./in.)	Maximum axial strain (in./in.)
25	4LR#3@1.5	304.8	9.18	0.00694	0.00661
26		289.38	8.72	0.00694	0.0072
27	6LR#3@1.5	365.68	11.02	0.0208	0.0138
28		353.76	10.66	0.0145	0.013

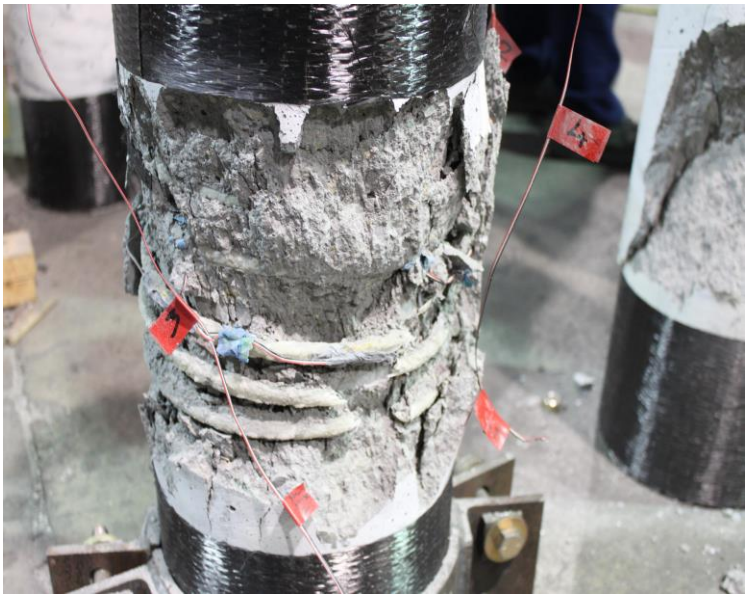

Figure 3.1: Concrete prism reinforced with GFRP spiral #3@1.5 at failure.

Figure 3.2: Concrete prism reinforced with GFRP spiral #3@2 at failure.

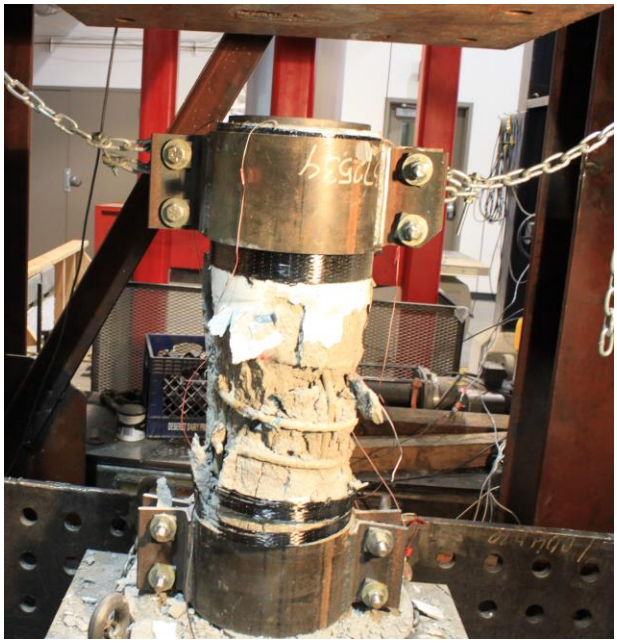

Figure 3.3: Concrete prism reinforced with GFRP spiral #3@3 at failure.

Figure 3.4: Concrete prism reinforced with GFRP spiral #4@1.5 at failure.

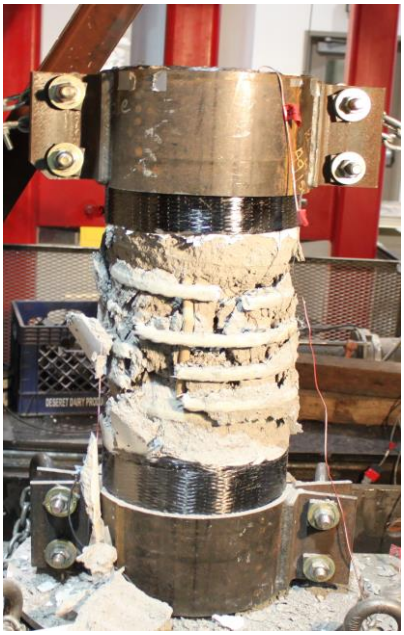

Figure 3.5: Concrete prism reinforced with GFRP spiral #4@2 at failure.

Figure 3.6: Concrete prism reinforced with GFRP spiral #5@1.5 at failure.

Figure 3.7: Concrete prism reinforced with GFRP spiral #5@2 at failure.

Figure 3.8: Concrete prism reinforced with GFRP spiral #5@2.5 at failure.

Figure 3.9: Failure of plain concrete prisms without any reinforcement.

Figure 3.10: GFRP reinforced concrete column 4LR#3@1.5 at failure.

Figure 3.11: GFRP reinforced concrete column 6LR#3@1.5 at failure.

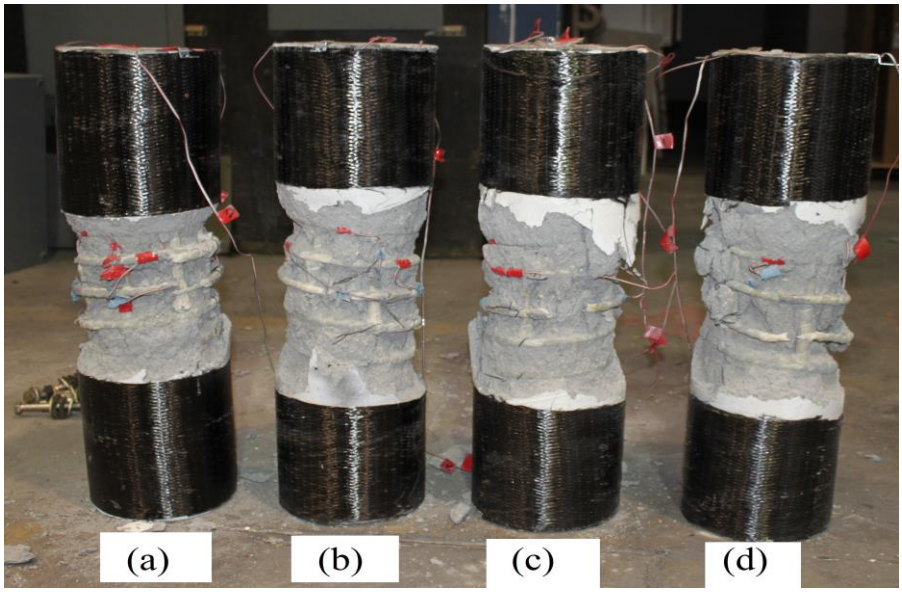

Figure 3.12: Failure of all four concrete columns (a) 6LR#3@1.5; (b) 6LR#3@1.5; (c) 4LR#3@1.5; (d) 4LR#3@1.5.

CHAPTER 4

ANALYTICAL CONFINEMENT MODEL FOR CONCRETE COLUMNS REINFORCED WITH GFRP SPIRALS

The analytical process of developing equations for the compressive strength of confined concrete (f'_{cc}) and ultimate axial compressive strain (ε_{ccu}) is described in this chapter. The most common way of analyzing the performance of confined concrete under axial load is the stress-strain curve. The stress-strain curve is an important property for both analysis and design of concrete columns.

The experimental stress-strain curves of representative specimens from the compressive load test are shown in Figures 4.1 to 4.10. The experimental curves show axial stress versus both axial strain and hoop strain. One specimen from each type was selected which represents the stress-strain curve of the specimen type. All stress-strain curves clearly show the nonyielding property of the GFRP composites spirals.

Column ductility was found for the four GFRP reinforced concrete columns. The column ductility is defined based on the displacement as at an axial load, which is equal to 85% of peak axial load. The column ductility (μ) is obtained by the following equation.

$$\mu = \frac{\Delta_{85}}{\Delta_1} \tag{4.1}$$

where Δ_{85} = displacement that corresponds to axial load which is 85% of peak axial load and Δ_1 = displacement that corresponds with limit of the elastic behavior. These values of displacements were obtained from load-displacement curves which are shown from Figures 4.11 to 4-14. A best fit line to the linear segment of these load-displacement curves was extended to intersect the maximum load (P_{max}), the displacement at this point of intersection was considered as Δ_1. The results of column ductility are shown in Table 4.1. The column ductility ranges from 2.25 to 4.36.

4.1 Basic parameters needed for the confinement model

To develop and validate the confinement model according to the guidelines of ACI 440.2R-08, the following basic parameters are required: (1) maximum confining pressure due to GFRP spirals (f_l); (2) compressive strength of unconfined concrete (f'_{co}); (3) slope of linear portion of stress-strain for FRP confined concrete (E_2); (4) modulus of elasticity of unconfined concrete (E_c); (5) maximum strain of unconfined concrete (ε'_c); (5) effective strain level in GFRP reinforcement attained at failure (ε_{fe}); and (6) confinement effectiveness k_e.

The value of confining pressure varies with respect to the area and modulus of the GFRP spiral, the pitch of the GFRP spiral and the hoop strain of the GFRP spirals at failure. The confining pressure for each specimen was calculated using the following equation:

$$f_l = k_e \frac{2E_{frp}\varepsilon_{fe}A_{frp}}{sD'} \qquad (4.2)$$

where E_{frp} = FRP composite tensile modulus, ε_{ke} = strain achieved by FRP spirals at failure, A_{frp} = cross-sectional area of the FRP spiral, s = pitch between the spirals, D` = diameter

of the area loaded and k_e = confinement effectiveness which can be found using equation (4.3). For ε_{fe}, the hoop strain values which were obtained from the strain gauges at the failure of the specimens were used. This can be justified using equation $\varepsilon_{fe} = k_{\varepsilon}.\varepsilon_{fu}$ where ε_{fu} = ultimate hoop strain value of the GFRP spiral shown in Table 2.3 and k_ε is the FRP efficiency factor.

The average value of k_ε calculated from the test data obtained was 0.62 and the standard deviation for k_ε was 0.14. This value of k_ε is close to 0.55 which is suggested in ACI 440.2R-08 for FRP jackets.

$$k_e = 1 - \frac{s`}{2D_s} = 1 - \left(\frac{s - d_{frp}}{2D_s} \right) \tag{4.3}$$

where d_{frp} = diameter of FRP spiral and D_s = effective diameter of concrete as shown in Figure 4.15. The values for confining pressure and confinement effectiveness for each specimen are tabulated in Table 4.2. The value of k_e takes into consideration the ineffective part of the core concrete. To consider this ineffective core on concrete, the pitch is considered as s` as shown in Figure 4.15. and s` given by ($s - d_{frp}$).

4.2 Model for compressive strength of confined concrete

The confinement model provides a general equation to calculate the capacity of a concrete column confined with GFRP spirals under pure axial compression. To obtain this equation, a graph of strengthening ratio (f'_{cc}/f'_{co}) against actual confinement (f_l/f'_{co}) is plotted. Here f'_{co} was used as 7.2 ksi, obtained as the average compressive strength of 4x8 cylinders on the day of the tests. Confined concrete strength f'_{cc} is obtained by dividing the load at failure with the loaded cross-sectional area of concrete that was loaded; the values

for f'_{cc} are tabulated in Table 2.1 for concrete prisms and Table 2.2 for concrete columns. The plot of strengthening ratio against actual confinement ratio is shown in Figure 4.16. The trendline of this test data is given by the following equation:

$$\frac{f'_{cc}}{f'_{co}} = 0.85 + 1.37\frac{f_l}{f'_{co}} \tag{4.4}$$

Thus, the compressive strength of the confined concrete can be calculated using the following equation:

$$f'_{cc} = 0.85 f'_{co} + 1.37 f_l \tag{4.5}$$

The R^2 value for the test data of strengthening ratio versus actual confinement ratio is 0.7993. The trendline provides a commonly used factor of 0.85 for f'_{co}, which indicates that there is a reduction in compressive strength of concrete for a structure with a significant size.

When the graph of strengthening ratio versus actual confinement is compared with results from other similar specimens from the literature, it is observed that the actual confinement values for concrete prisms were higher. This was mainly because of the higher confinement pressure that was achieved in the concrete prisms. The higher confinement pressure was achieved with the help of wooden dowels that were used to hold the spirals at the required pitch. The wooden dowels were less stiff than the GFRP bars which allowed the spirals to reach close to their tensile strain capacity. The strengthening ratio and the actual confinement ratio for concrete columns of the literature are shown in Table 4.4. From the test data, it is observed that a higher strengthening ratio was obtained for higher values of the actual confinement ratio. Also for a particular actual confinement ratio, the strengthening ratio of the concrete columns is about 60% more than the concrete prisms.

4.3 Model for ultimate axial compressive strain of confined concrete

To obtain the model for ultimate compressive strain of confined concrete, it is required to plot the graph of strain enhancement ($\varepsilon_{ccu}/\varepsilon'_c$) against quantity X_o, where X_o is given by equation (4.5).

$$X_o = \left(\frac{2E_{frp}A_{frp}}{E_{sec}sD'}\right)\left(\frac{\varepsilon_{h,rup}}{\varepsilon'_c}\right)^{\beta} \tag{4.6}$$

where E_{sec} is the secant modulus of elasticity at the compressive strength of unconfined concrete and is given by f'_{co}/ε'_c. The value of β is found by performing iterations of the test data to obtain a suitable R^2 value. The plot is shown in Figure 4.17. For the purpose of plotting the graph, ε_{ccu} was considered as the axial strain obtained from the LVDTs for the concrete prisms. According to ACI 440.2R-08, the value of ε'_c can be taken as 0.002. After performing iterations of the test data, the value of β was obtained as 1.15. The trendline of the above plot can be approximated with the following equation:

$$\frac{\varepsilon_{ccu}}{\varepsilon'_c} = 2.4 + 5.6\left(\frac{2E_{frp}A_{frp}}{E_{sec}sD'}\right)\left(\frac{\varepsilon_{h,rup}}{\varepsilon'_c}\right)^{1.15} \tag{4.7}$$

Thus the ultimate axial compressive strain of the confined concrete can be expressed as:

$$\varepsilon_{ccu} = \varepsilon'_c\left(2.4 + 5.6\frac{f_l}{f'_{co}}\left(\frac{\varepsilon_{h,rup}}{\varepsilon'_c}\right)^{0.15}\right) \tag{4.8}$$

To prevent excessive cracking and resulting in loss of concrete integrity, the value of ultimate axial compressive strain of the confined concrete should be limited to a

particular value. This value was decided by finding the ε_{ccu} values of concrete prisms using equation (4.8); the maximum of these values was 0.0142 in./in. Thus, to be conservative, the value of ε_{ccu} was limited to 0.014 in. /in.

$$\varepsilon_{ccu} \leq 0.014 \tag{4.9}$$

4.4 Validation of the confinement model

The confinement model based on the prism tests was validated by using equations (4.5) and (4.8) and the stress-strain curves from the four concrete columns tested in this study, two specimens from Pantelides et al. (2013) and one specimen from Hales (2015). These calculated stress-strain curves were compared with the stress-strain curves obtained from the test conducted on these specimens.

The specimens selected form Pantelides et al. (2013) were #13GLCTL and #14 GLCTL. These specimens were constructed with all-GFRP reinforcement. The columns had a diameter of 10 in. and height of 28 in. The concrete used for these specimens had a compressive strength of 5.2 ksi. The columns were reinforced with four #5 GFRP longitudinal bars and #3 GFRP spirals with the pitch of 3 in. The specimen selected from Hales (2015) was named #3S-SG0. The column had a diameter of 12 in. and height of 30 in. The compressive strength of the concrete used to build this column was 13 ksi. The column was reinforced with six #5 longitudinal bars and #3 spirals with pitch of 3 in.

To obtain the values for axial stress (f_c) versus axial strain (ε_c), the following equations are used:

$$f_c = E_c\varepsilon_c - \frac{(E_c - E_2)^2}{4f'_{co}}\varepsilon_c^{\,2} \quad \text{when } 0 \leq \varepsilon_c \leq \varepsilon'_t \tag{4.10}$$

$$f_c = f'_{co} + E_2\varepsilon_c \qquad \text{when } \varepsilon'_t < \varepsilon_c \le \varepsilon_{ccu} \tag{4.11}$$

$$E_2 = \frac{f'_{cc} - \left(0.85 f'_{co}\right)}{\varepsilon_{ccu}} \tag{4.12}$$

$$\varepsilon'_t = \frac{2 f'_{co}}{E_c - E_2} \tag{4.13}$$

The above equations were obtained from ACI 440.2R-08. A generic stress-strain curve for unconfined and confined concrete is shown in Figure 4.18. The values of f'_{cc} and ε_{ccu} were calculated using equations (4.5) and (4.8). The modulus of elasticity of concrete E_c is given as $57000\sqrt{f'_{co}}$ lb/in^2. The parameters required to plot the stress-strain curves are given in Table 4.3. A comparison between the stress-strain curves obtained by equation and experimentally is shown in Figure 4.19 – Figure 4.25. After comparing the stress-strain curves, it was observed that the value of compressive strength of the confined concrete using equation (4.5) is slightly less than f'_{cc} obtained from the experiments for six out of seven specimens. Similarly, the ultimate axial compressive strain achieved during the experiment is higher than the strain obtained by equation (4.8) for five out of seven specimens. This indicates that the model developed for the compressive strength and ultimate axial compressive strain of confined concrete is conservative for design purposes. The value of ultimate axial compressive strain obtained from the test results for specimen #3S-SG0 was lower than the predicted value. This was mainly because the concrete used for #3S-SG0 was a high-strength concrete having compressive strength of 13,000 psi.

Table 4.1: Column ductility for GFRP reinforced concrete columns.

Column Specimen	Peak axial load (P_{max}) (kips)	85% of Pmax (kips)	Δ_1 (in.)	Δ_{85} (in.)	Column ductility (μ)
4LR#4@1.5(1)	304.8	259.08	0.0595	0.134	2.25
4LR#4@1.5(2)	289.38	245.973	0.041	0.179	4.36
6LR#4@1.5(1)	365.68	310.828	0.085	0.27	3.17
6LR#4@1.5(2)	353.76	300.696	0.0856	0.254	2.97

Table 4.2: Basic parameters required for confinement model of compressive strength of prism.

Specimen No.	Specimen type	k_e [Eq. (4.2)]	f_l (ksi)	f_l/f'_{co}	f'_{cc}/f'_{co}
1	#3@1.5	0.94	1.182	0.164	1.108
2		0.94	1.509	0.209	1.203
3		0.94	1.356	0.188	1.245
4	#3@2	0.914	0.839	0.116	0.98
5		0.914	0.631	0.087	1.031
6		0.914	0.727	0.101	0.984
7	#3@3	0.861	0.725	0.101	0.812
8		0.861	0.648	0.090	0.956
9		0.861	0.676	0.094	0.822
10	#4@1.5	0.947	1.828	0.254	1.226
11		0.947	2.916	0.405	1.303
12		0.947	1.987	0.276	1.281
13	#4@2	0.921	1.728	0.240	1.101
14		0.912	1.88	0.261	1.146
15		0.921	1.75	0.243	1.105
16	#5@1.5	0.953	4.471	0.621	1.693
17		0.953	3.96	0.550	1.609
18		0.953	2.052	0.285	1.537
19	#5@2	0.927	3.506	0.487	1.429
20	#5@2.5	0.901	1.56	0.218	1.168
21		0.901	1.137	0.158	1.168

Table 4.3: Parameters to plot the stress-strain curves for GFRP reinforced concrete columns.

Specimen	f_l/f'_{co}	f_l (ksi)	f'_{cc} (ksi)	ε_{ccu} (in./in.)	E_2	ε'_t (in/in)
4LR#3@1.5(1)	0.103	0.742	8.215	0.00627	161.86	0.00308
4LR#3@1.5(2)	0.103	0.742	8.215	0.00627	161.86	0.00308
6LR#3@1.5(1)	0.309	2.226	10.246	0.0098	310.66	0.00318
6LR#3@1.5(2)	0.215	1.553	9.324	0.00813	261.19	0.00314
#13GLCTL	0.011	0.0608	5.283	0.005	16.64	0.00254
#14GLCTL	0.018	0.0936	5.328	0.0051	25.203	0.00254
#3S-SG0	0.0028	0.037	13.05	0.0049	10.335	0.004

Table 4.4: Comparison of confinement model for similar kind of specimens in literature.

Authors	Specimen	ρ_v (%)	ρ_t (%)	f'_{co} (ksi)	f_l/f'_{co}	f'_{cc}/f'_{co}	f'_{cc} (experi-mental) (ksi)	f'_{cc} (model) (ksi)
Current study	4LR#4@1.5(1)	2.46	3.33	7.2	0.103	1.758	9.18	8.29
	4LR#4@1.5(2)	2.46	3.33	7.2	0.103	1.670	8.72	8.29
	6LR#4@1.5(1)	3.70	3.33	7.2	0.309	2.109	11.02	10.49
	6LR#4@1.5(2)	3.70	3.33	7.2	0.215	2.041	10.36	9.49
Pantelides et al. (2013)	#13GLCTL	1.50	1.70	5.2	0.008	1.087	5.64	5.28
	#14GLCTL	1.50	1.70	5.2	0.012	0.984	5.11	5.09
Hales (2016)	#3S-SG0	1.60	1.70	13	0.002	1.089	14.11	13.05
Afifi et al. (2015)	C10V-3H80	1.70	1.70	6.2	0.075	1.29	7.99	5.90
	C6V-3H80	2.20	1.70	6.2	0.059	1.24	7.68	5.77
	C14V-3H80	1.10	1.00	6.2	0.082	1.39	8.61	5.96
	C10V-2H80	3.20	2.40	6.2	0.036	1.19	7.37	5.57
	C10V-4H80	2.20	1.70	6.2	0.131	1.37	8.49	6.38
	C10V-3H40	2.20	1.70	6.2	0.214	1.37	8.49	7.08
	C10V-3H120	2.20	1.70	6.2	0.035	1.22	7.56	5.56
	C10V-2H35	2.20	1.70	6.2	0.116	1.45	8.99	6.25
	C10V-4H145	2.20	1.70	6.2	0.042	1.24	7.68	5.62
	C10V-3O200	2.20	1.70	6.2	0.044	1.05	6.51	5.64
	C10V-3O400	2.20	1.70	6.2	0.059	1.12	6.94	5.77
	C10V-3O600	2.20	1.70	6.2	0.074	1.21	7.50	5.89

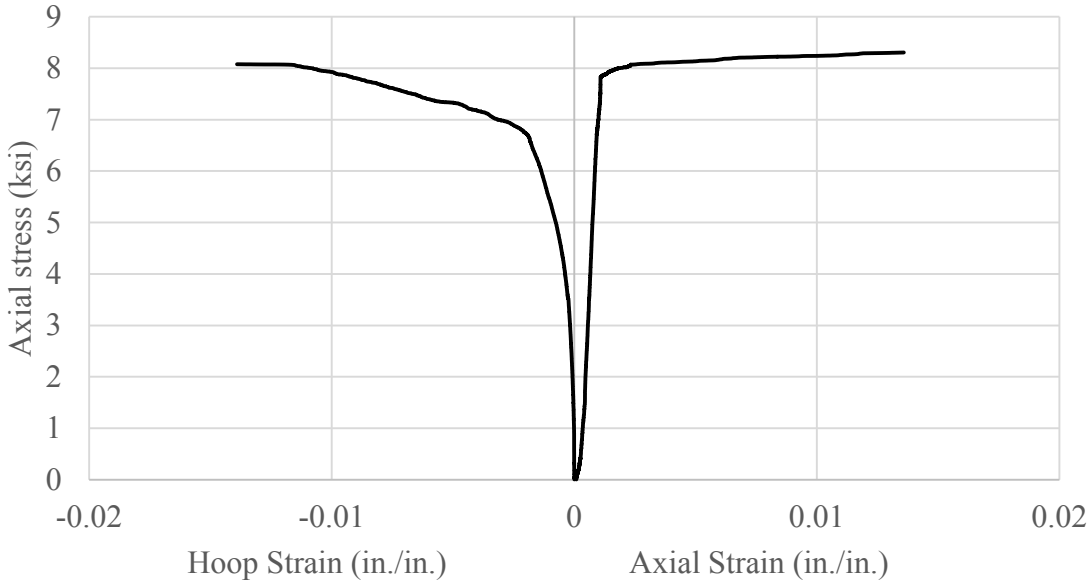

Figure 4.1: Experimental stress-strain curve of concrete prism #3@1.5.

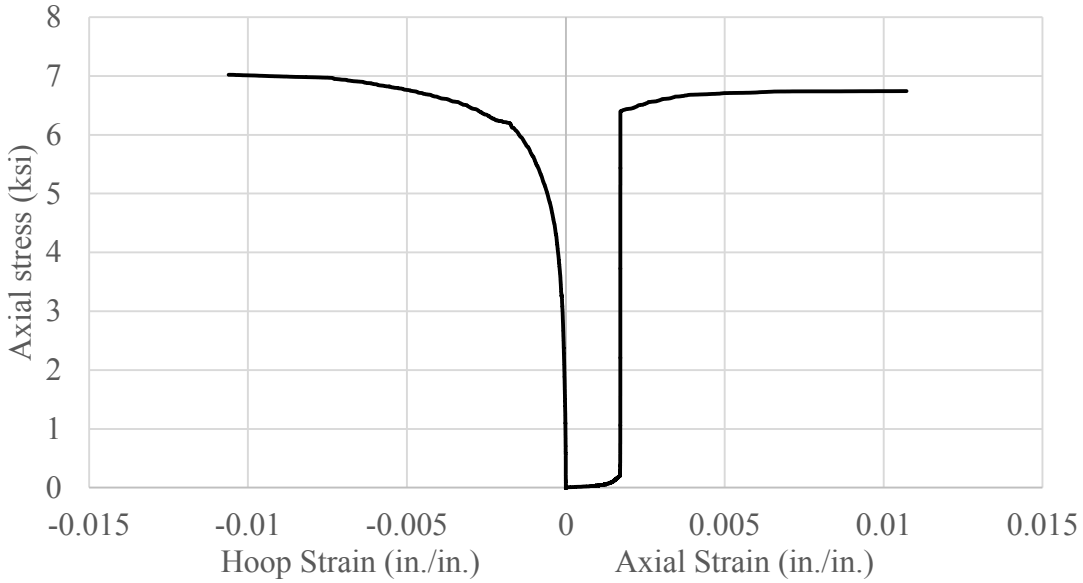

Figure 4.2: Experimental stress-strain curve concrete prism of #3@2.

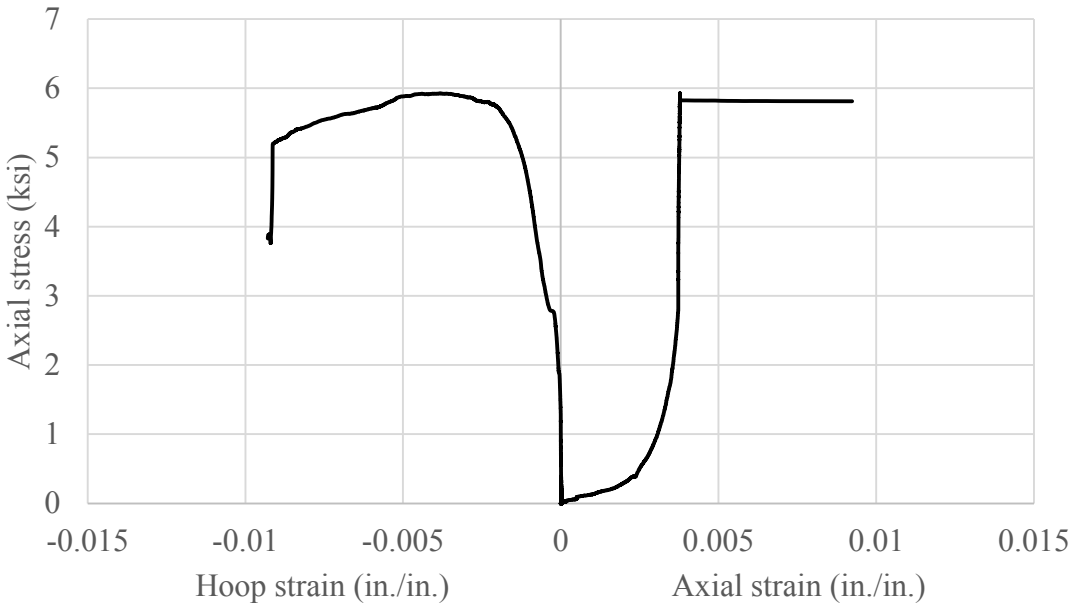

Figure 4.3: Experimental stress-strain curve of concrete prism #3@3.

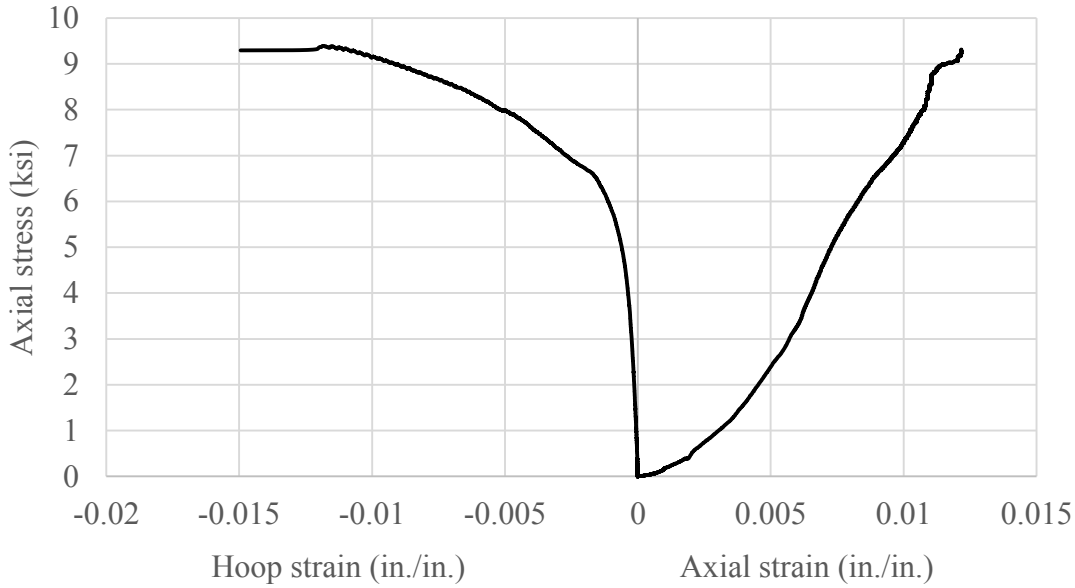

Figure 4.4: Experimental stress-strain curve of concrete prism #4@1.5.

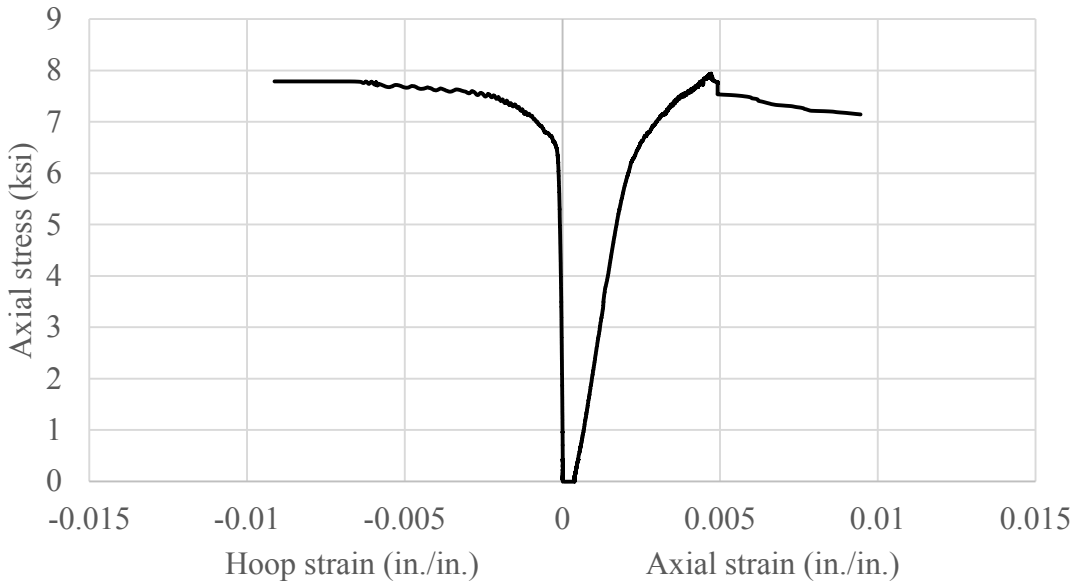

Figure 4.5: Experimental stress-strain curve of concrete prism #4@2.

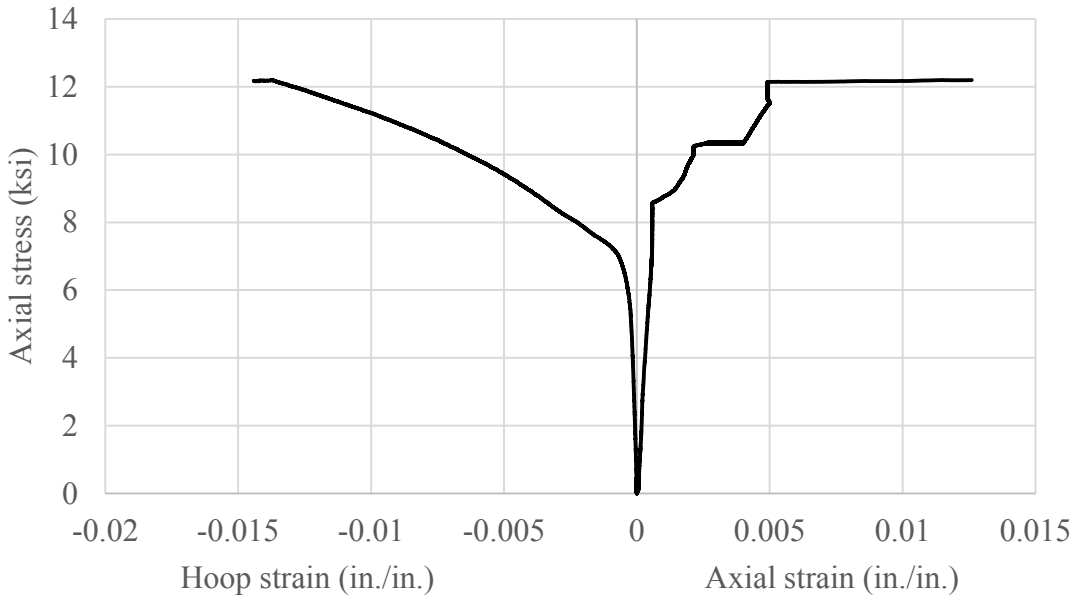

Figure 4.6: Experimental stress-strain curve of concrete prism #5@1.5

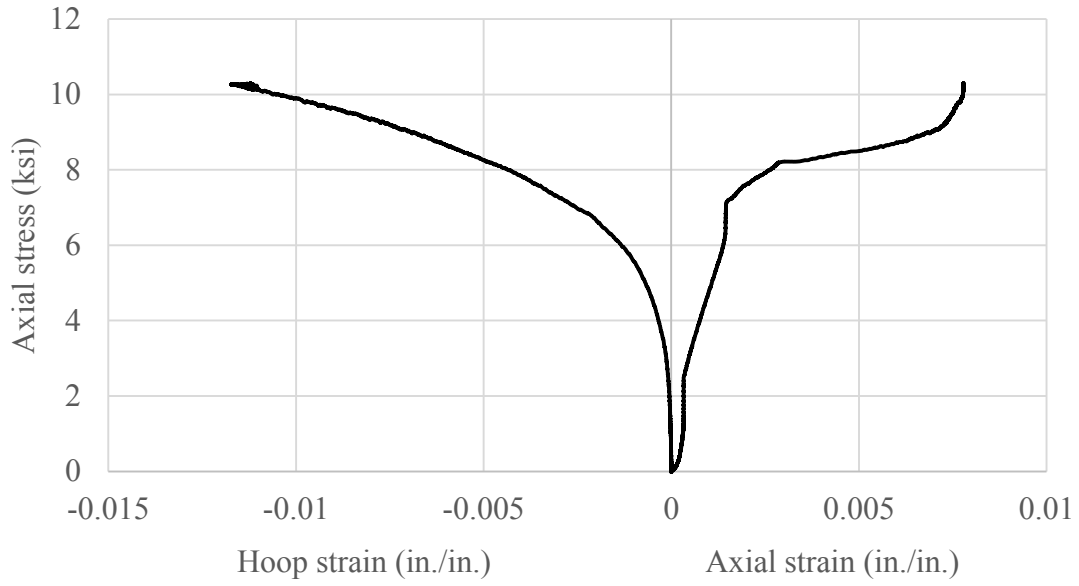

Figure 4.7: Experimental stress-strain curve for concrete prism #5@2.

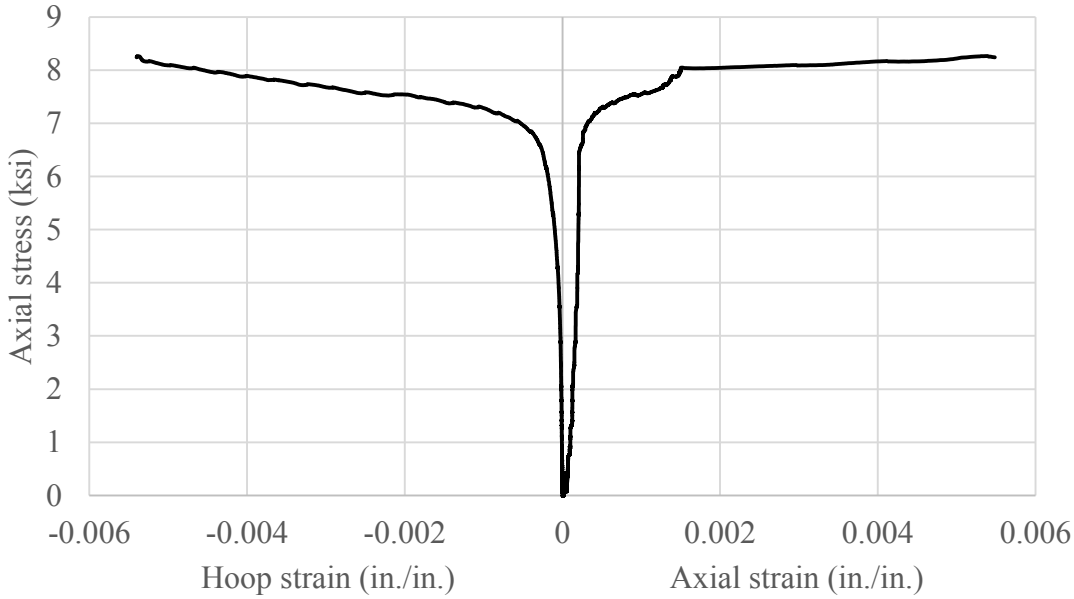

Figure 4.8: Experimental stress-strain curve of concrete prism #5@2.5.

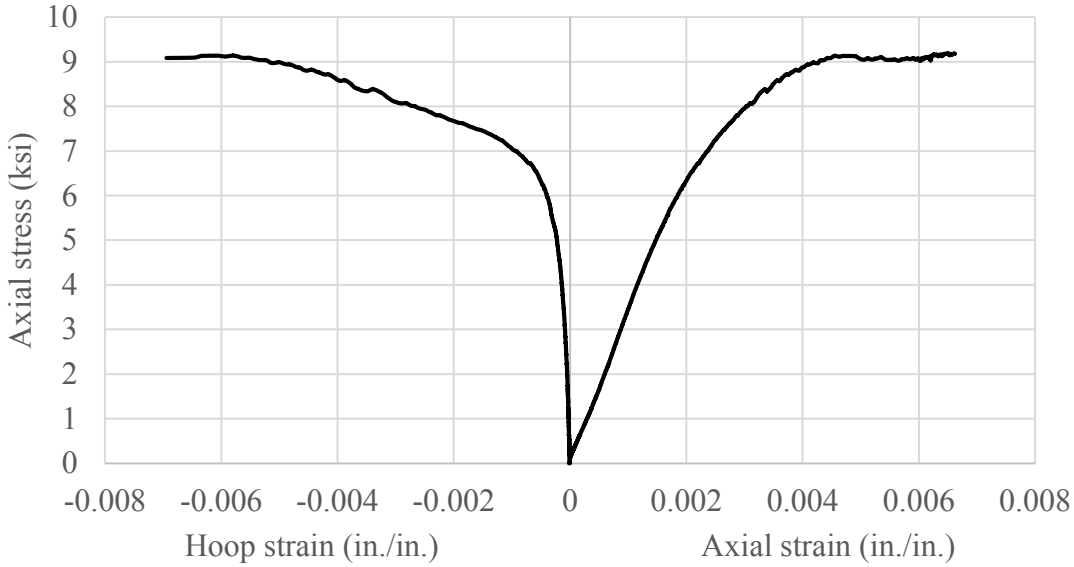

Figure 4.9: Experimental stress-strain curve of GFRP reinforced concrete column 4LR#3@1.5.

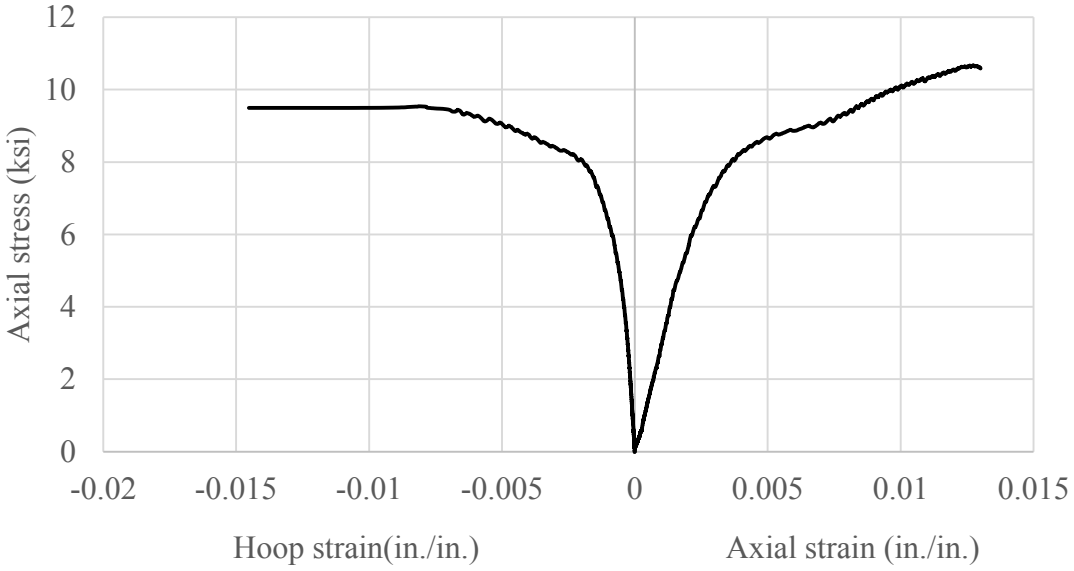

Figure 4.10: Experimental stress-strain curve of GFRP reinforced concrete column 6LR#3@1.5.

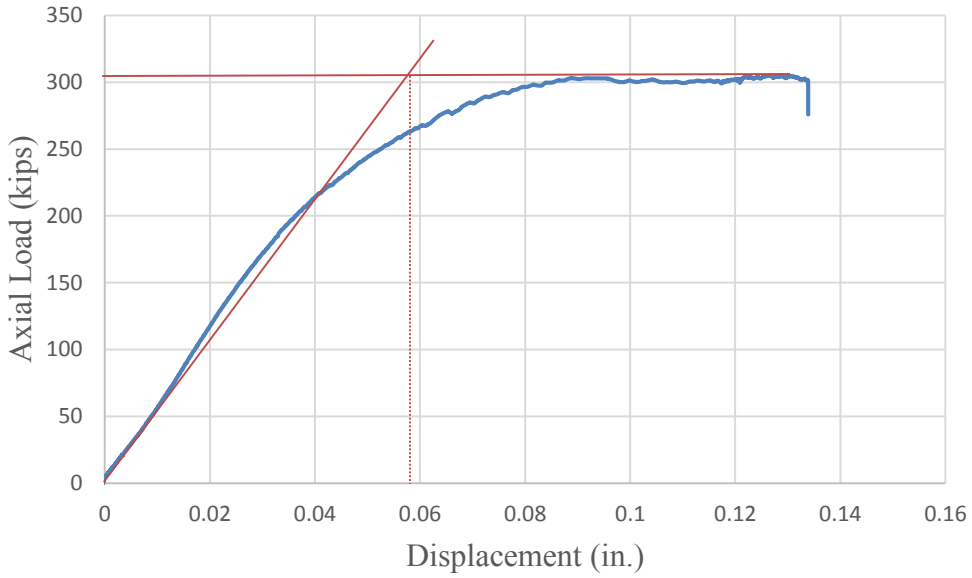

Figure 4.11: Load-displacement curve of 4LR#3@1.5 (1)

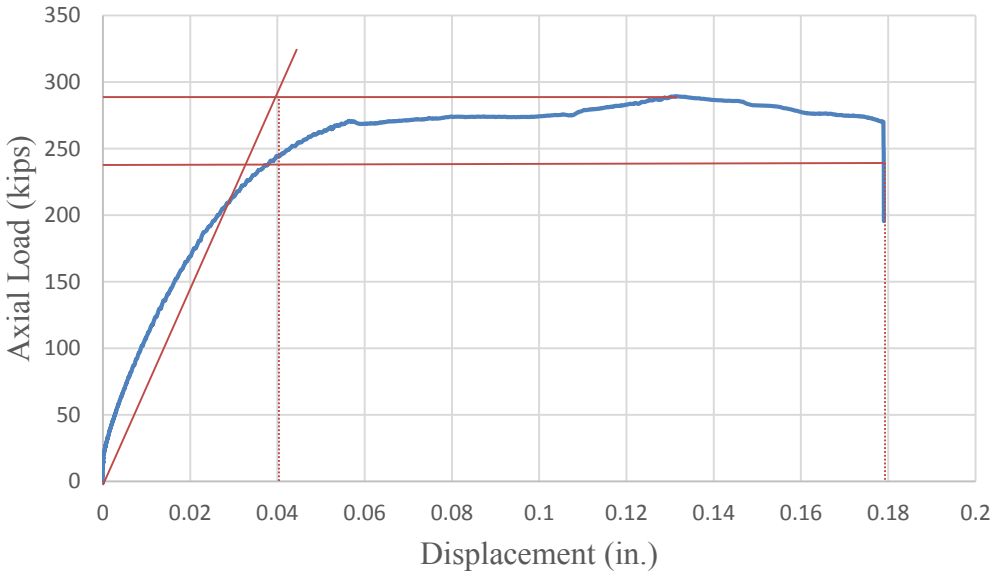

Figure 4.12: Load-displacement curve of 4LR#3@1.5 (2)

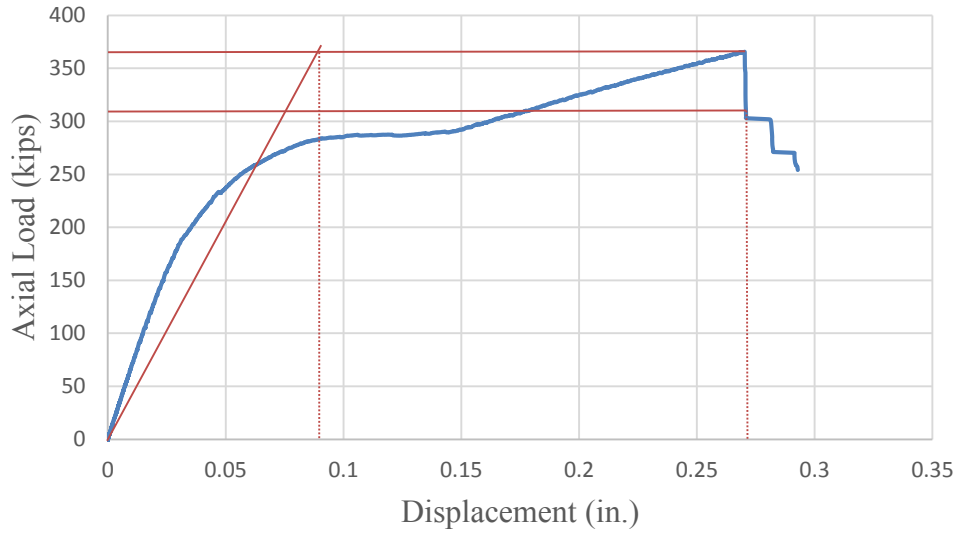

Figure 4.13: Load-displacement curve of 6LR#3@1.5 (1)

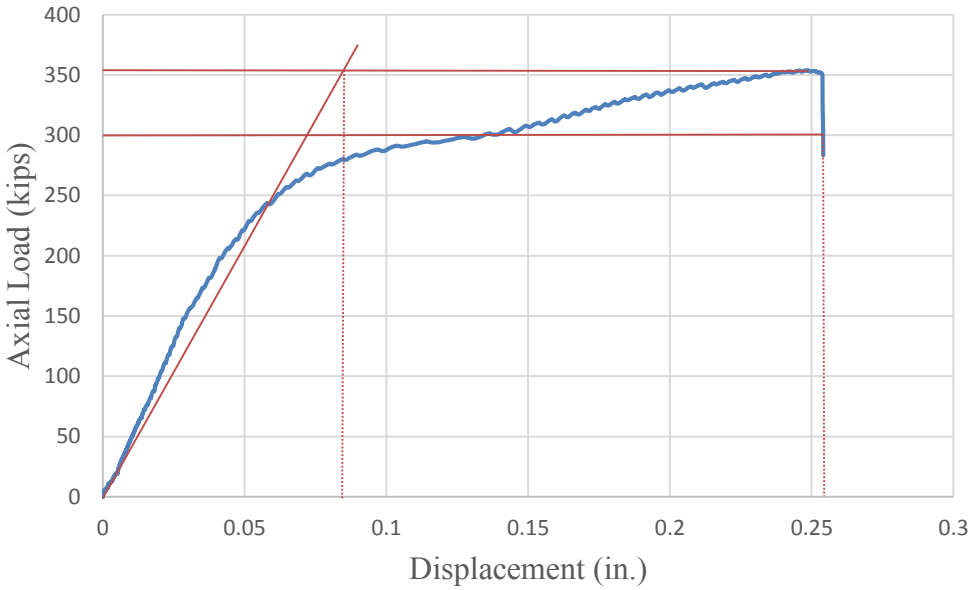

Figure 4.14: Load-displacement curve of 6LR#3@1.5 (2)

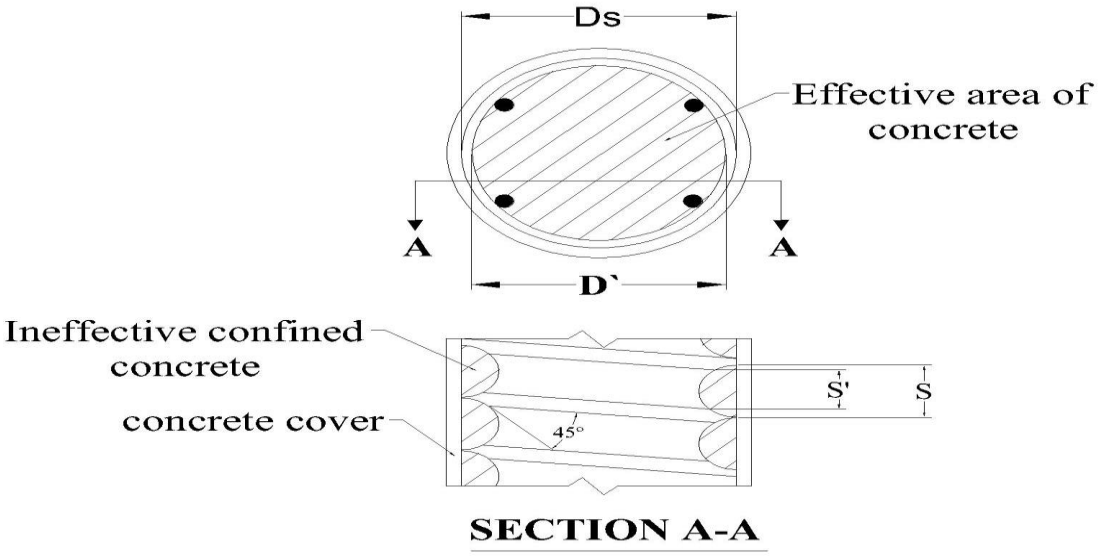

Figure 4.15: Effectively confined core for spiral reinforcement.

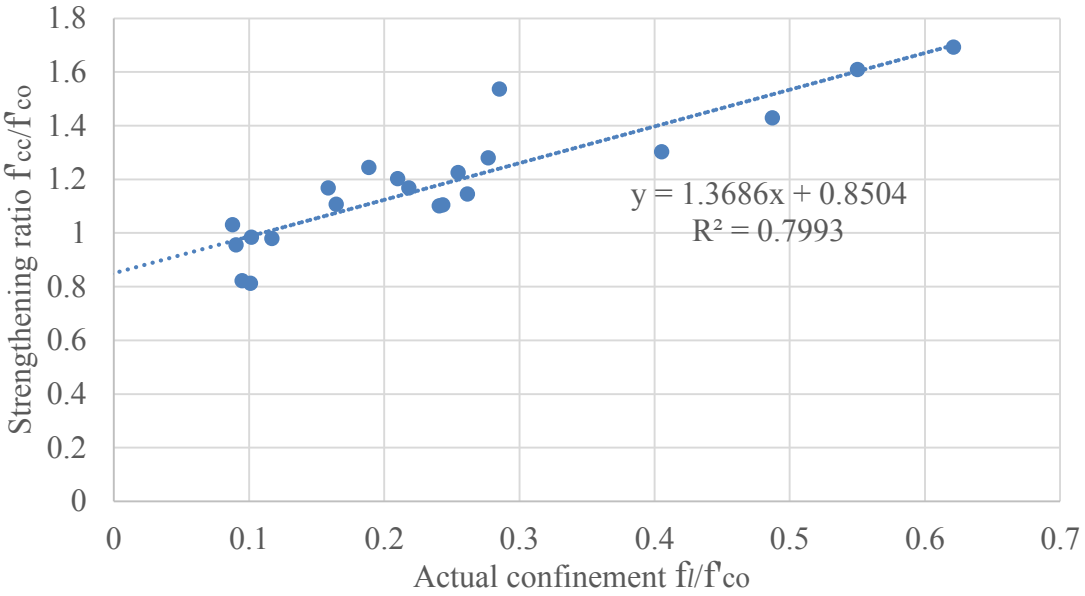

Figure 4.16: Plot of strengthening ratio against actual confinement for test data.

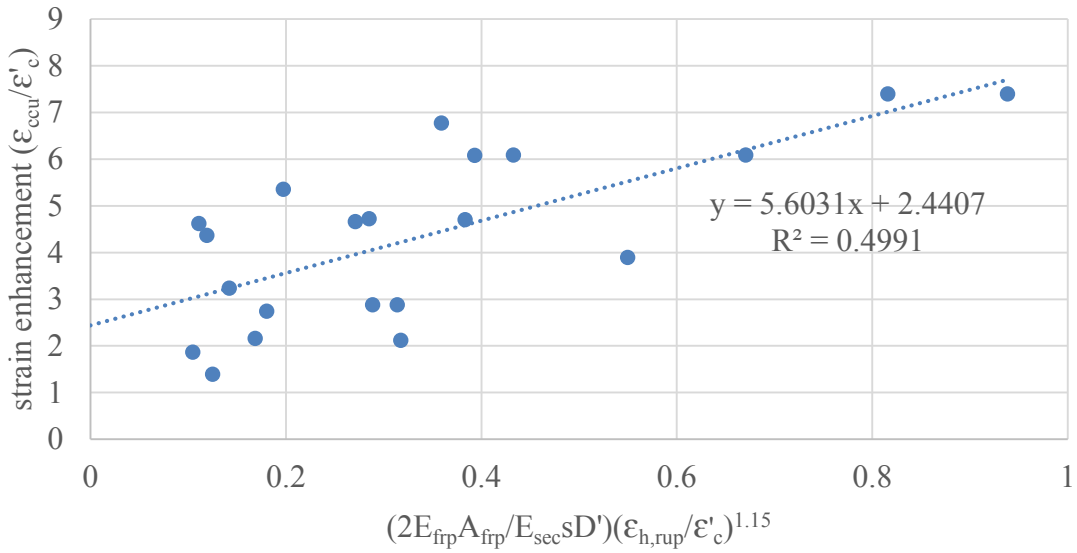

4.17: Plot to obtain equation for the ultimate axial compressive strain for confined concrete.

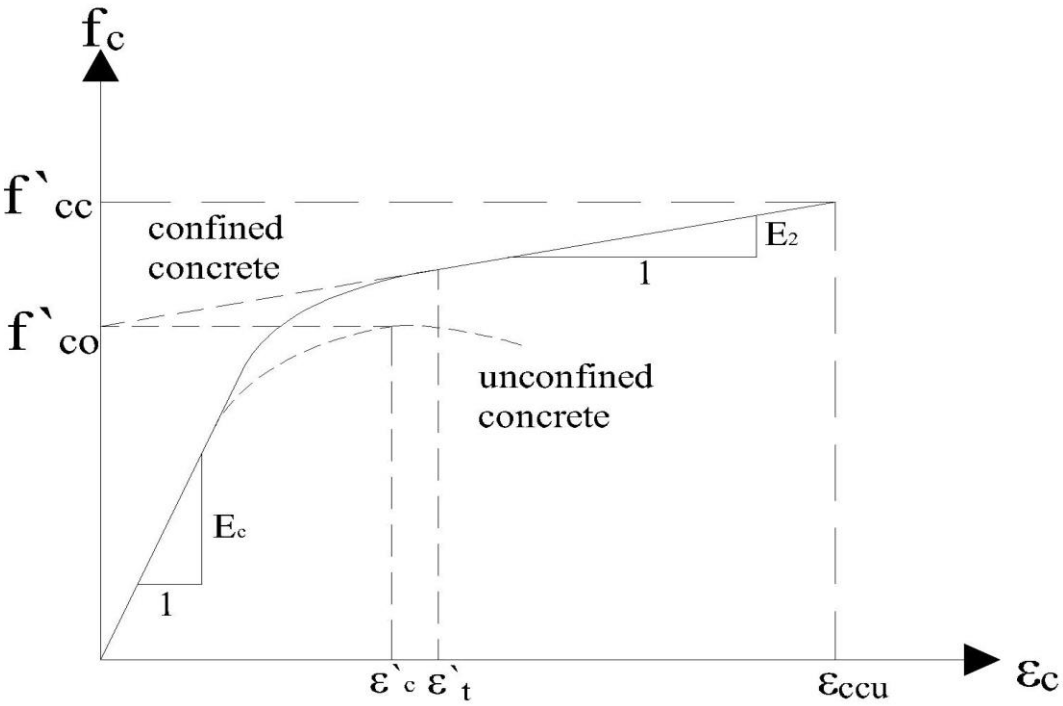

Figure 4.18: Generic stress-strain curve of unconfined and confined concrete.

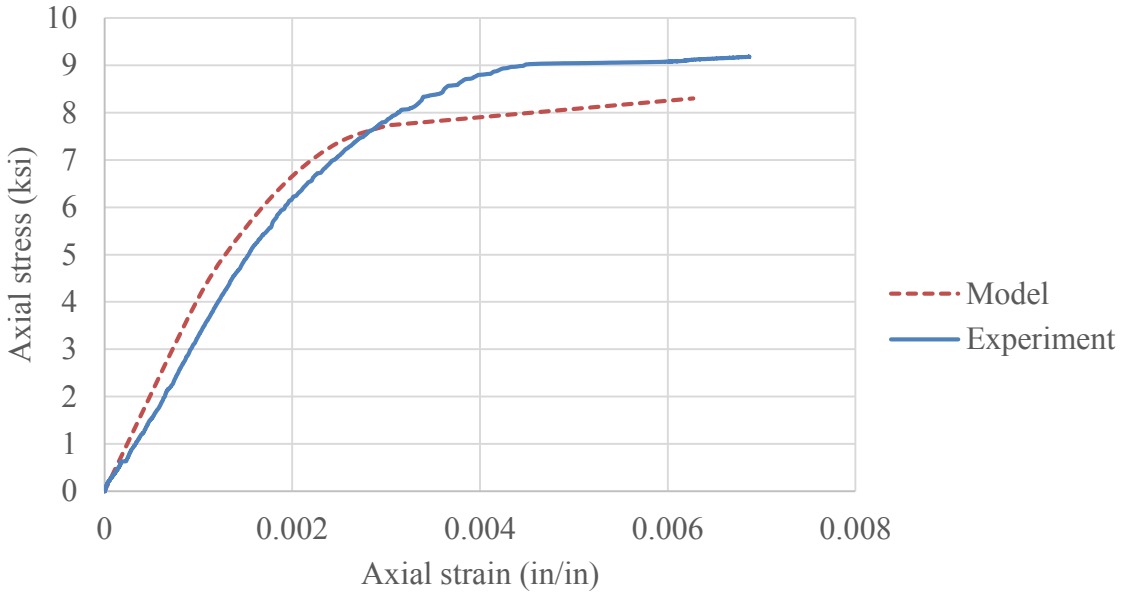

Figure 4.19: Comparison of stress-strain curve of 4LR#3@1.5 (1).

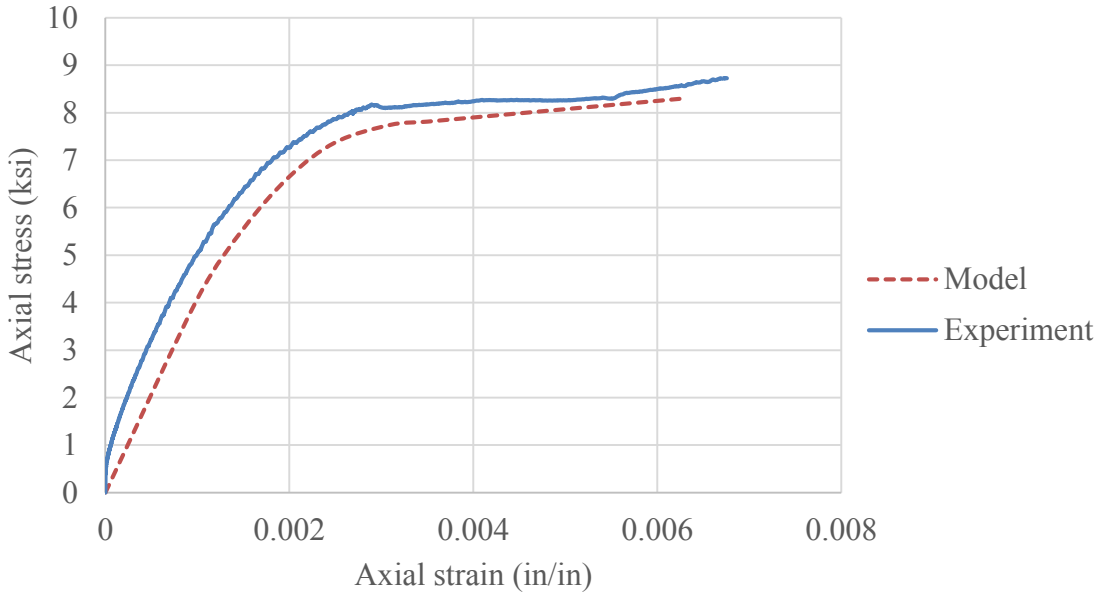

Figure 4.20: Comparison of stress-strain curve of 4LR#3@1.5 (2).

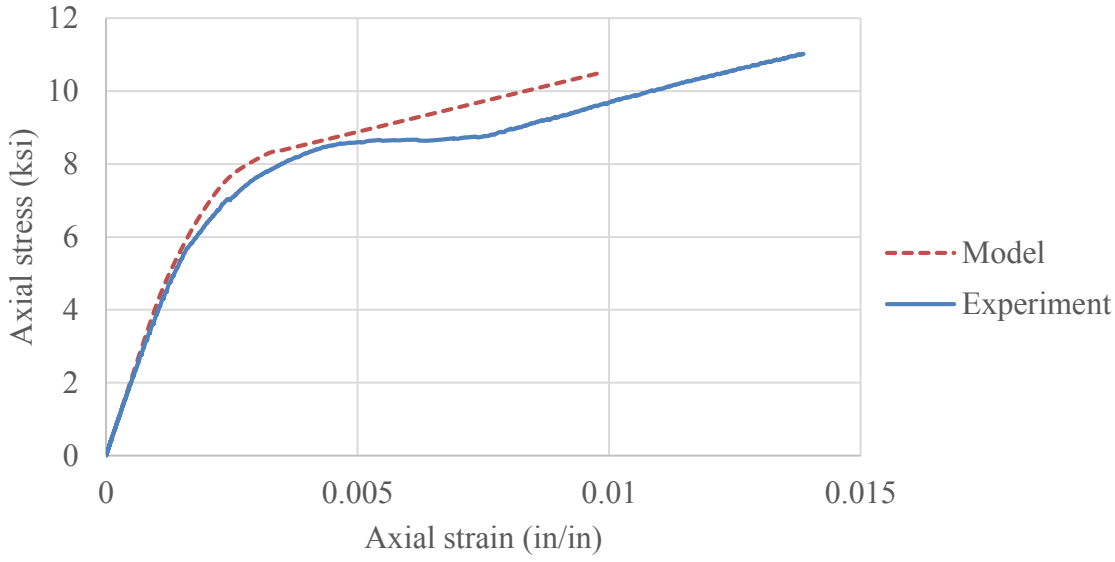

Figure 4.21: Comparison of stress-strain curve of 6LR#3@1.5 (1).

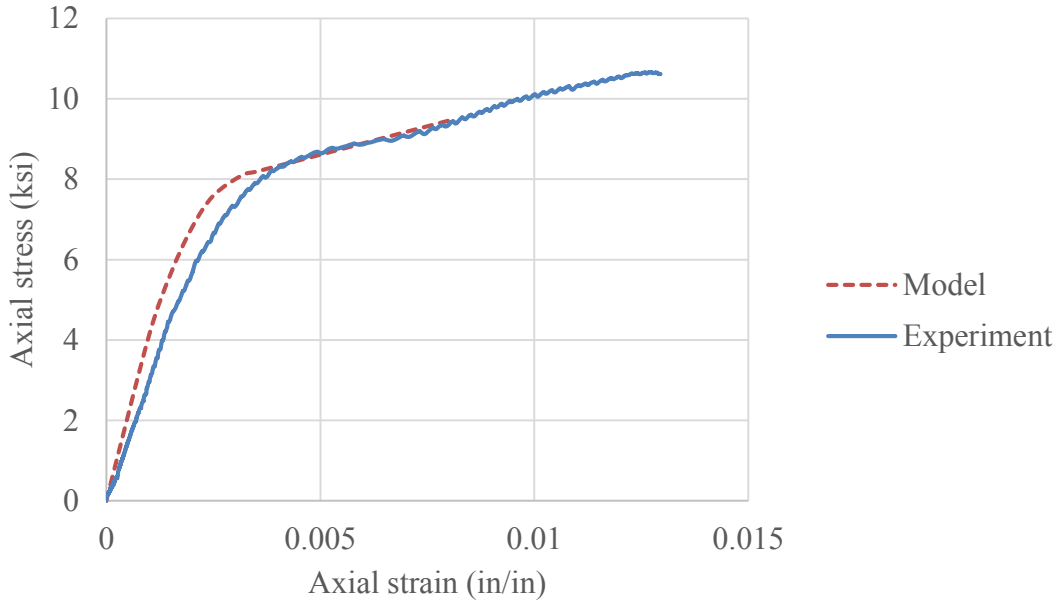

Figure 4.22: Comparison of stress-strain curve of 6LR#3@1.5 (2).

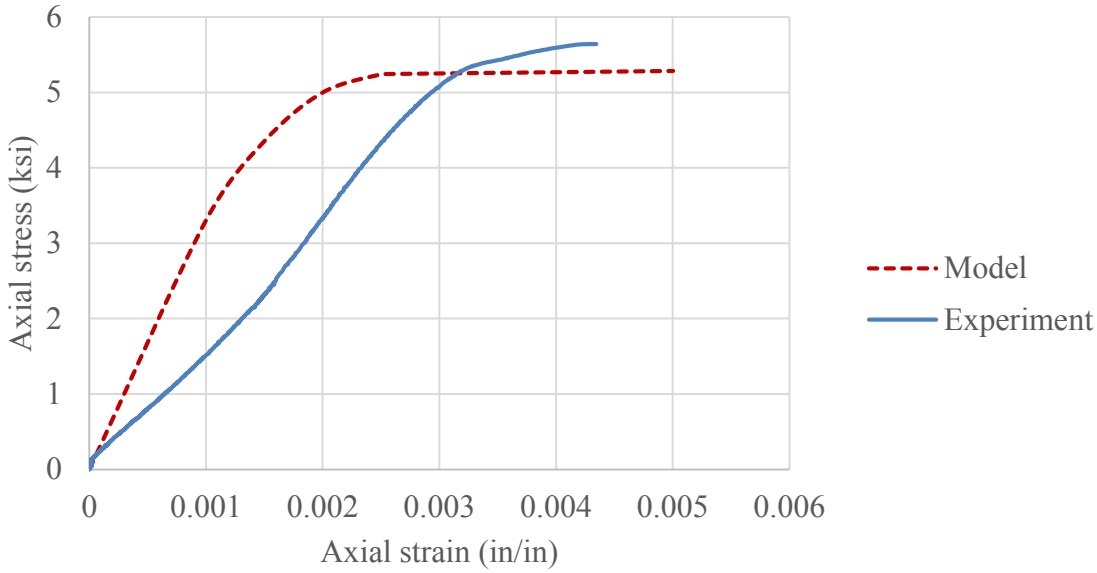

Figure 4.23: Comparison of stress-strain curve of #13GLCTL.

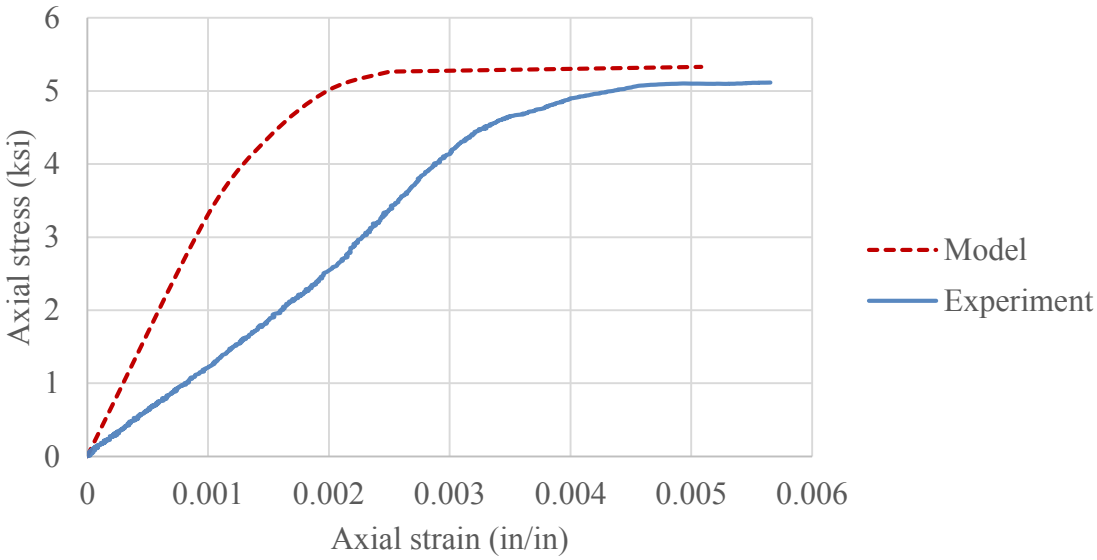

Figure 4.24: Comparison of stress-strain curve #14GLCTL.

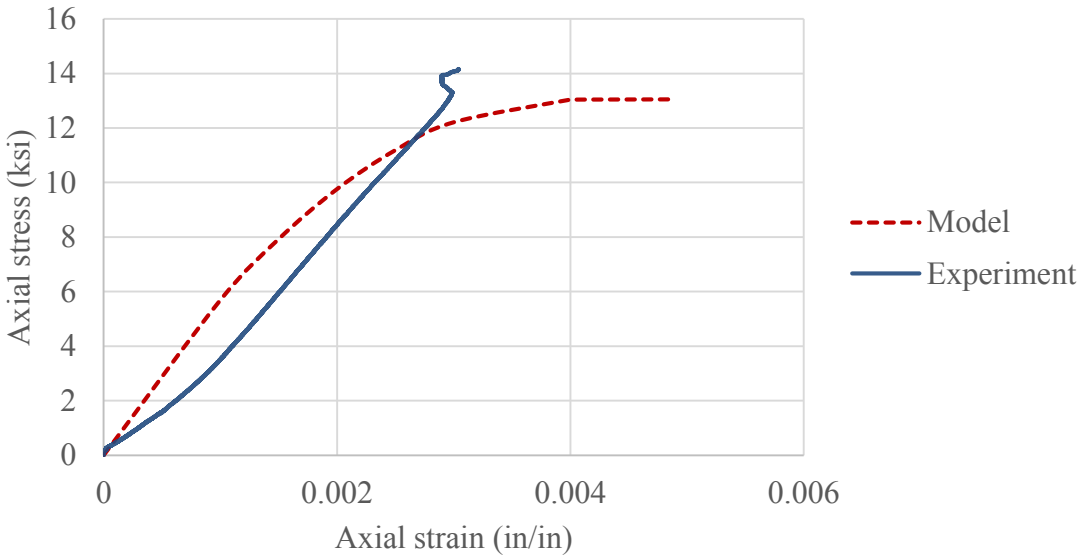

Figure 4.25: Comparison of stress-strain curve of #3S-SG0.

CHAPTER 5

CONCLUSIONS

Based on the experimental results and the analytical model developed in this research, the following conclusions are made:

1. To obtain higher confinement strength of concrete, GFRP spirals of bigger cross-sectional area be used with a lower pitch than the ones used in previous research. Due to the lower modulus of elasticity and elastic behavior of GFRP spirals, any lower cross-sectional areas and a larger pitch would provide a reduced effective confining pressure.
2. From concrete prisms confined with GFRP spirals, the confined strength of concrete was derived. While using this model, the minimum value of actual confinement ratio should be 0.1, i.e., $f_l / f'_{co} \geq 0.1$. No strength enhancement can be obtained for columns having actual confinement ratio smaller than 0.1.
3. The ultimate axial compressive strain of the concrete column was determined. This strain should be limited to a particular value, to prevent excessive cracking and loss of concrete integrity. The maximum value of ultimate compressive axial strain was based on ε_{ccu} values calculated for concrete prisms which gave the maximum value of 0.0142 in/in. Thus to be conservative, the maximum ultimate axial compressive strain should be limited to 0.014 in/in.

4. The ultimate hoop strain for well-confined prisms reinforced with GFRP spirals ranged from 0.010 in./in. to 0.0145 in./in. The ultimate hoop strain for well-confined concrete reinforced with GFRP spirals and GFRP longitudinal bars increases with increasing number of GFRP longitudinal bars.
5. The strength enhancement of concrete is higher for columns externally reinforced with FRP composites wraps than for concrete columns internally reinforced with FRP composites spirals. This can be concluded by comparing the analytical model obtained with similar equations in ACI 440.2R-08. In the equation for f'_{cc}, the coefficient for confining pressure for externally bonded FRP system is 3.3, while for concrete confined internally, it is 1.37. Thus the confining pressure for internally confined system is 58% less than the externally confined system.
6. Verification of the analytical model was done by comparing the stress-strain curve obtained by using equations and through the experiments. Thus it can be concluded that the equations developed for compressive strength and the ultimate axial compressive of confined concrete are conservative for design of concrete columns internally confined with GFRP spirals.

REFERENCES

ACI (American Concrete Institute) (2004). "Guide test methods for fiber-reinforced polymers (FRPs) for reinforcing or strengthening concrete structures." ACI 440.3R-04 Farmington Hills, MI.

ACI (American Concrete Institute) (2008). "Guide for design and construction of externally bonded FRP system for strengthening concrete structures." ACI 440.2R-08 Farmington Hills, MI.

Afifi, M. Z., Mohamed, H. M., and Benmokrane, B. (2015). "Theoretical stress strain model for circular concrete columns confined by GFRP spirals and hoop." *Engineering Structures* 102 (2015) 202-213.

Afifi, M. Z., Mohamed, H. M., Chaallal, O., and Benmokrane, B. (2015). "Confinement model for concrete columns internally confined with Carbon FRP spirals and Hoops." *J. Struct. Eng.* 2015.141.

Afifi, M. Z., Mohamed, H. M., and Benmokrane, B (2014). "Strength and axial behavior of circular concrete columns reinforced with CFRP bars and spirals." *J. Compos. Constr.* 2014.18.

Afifi, M. Z., Mohamed, H. M., and Benmokrane, B (2014). "Axial capacity of circular concrete columns reinforced with GFRP bars and spirals." *J. Compos. Constr.* 2014.18.

Alsayed, S. H., Al-Salloum, Y. A., Almusallam, T. H., and Amjad, M. A. (1999). "Concrete columns reinforced by glass fiber reinforced polymer rods." *Proc., Fourth Int. Symp. FRP Reinforcement for Reinf Conc. Struct., SP-188, C. W. Dolan, S. H. Rizkalla and A. Nanni, eds.,* American Concrete Institute, Farmington Hills, MI, 103-112.

De Luca, A., Matta, F., and Nanni, A. (2009). "Behavior of full-scale concrete columns internally reinforced with glass FRP bars under pure axial load." *Composites & Polycon 2009*, American Composites Manufactures Association, Tampa, FL, 1-10.

De Luca, A., Matta, F., and Nanni, A. (2010). "Behavior of full scale glass fiber-reinforced polymer reinforced concrete columns under axial load." *ACI Struct. J.,* 107(5), 589-596.

Hales, T. A., (2016). "Slender columns reinforced with fiber reinforced polymer spirals." Ph.D. dissertation, University of Utah, Salt Lake City.

Hogr, K., Sheikh, M. N., and Hadi, M. N. S. (2016). "Axial load – axial deformation behavior of circular concrete columns reinforced with GFRP bars and helices." *Construction and building materials.,* 112 (2016), 1147-1157.

Lam, L., and Teng, J.G. (2003). "Design-oriented stress-strain model for FRP-confined concrete." *Construction and building materials* 17 2003, 471-489.

Mander, J. B., Priestley, M. J. N., and Park, R. (1988). "Theoretical stress-strain model for confined concrete." *J. Struct. Eng.* 1988, 114(8): 1804-1826.

Mirmiran, A., Yuan, W., and Chen, X. (2001). "Design for slenderness in concrete columns internally reinforced with fiber-reinforced polymer bars." *ACI Struct. J.,* 98(1), 116-125.

Mohamed, H. M., Afifi, M. Z., and Benmokrane, B (2014). "Performance evaluation of concrete columns reinforced with longitudinally with FRP bars and confined with FRP hoops and spirals under axial load." *J. Bridge. Eng.* 2014.

Moran, D. A., Pantelides, C.P., (2012). "Elliptical and circular FRP-confined concrete sections: A Mohr-Coulomb analytical model." *International journal of solids and structures* 49 2012, 881-898.

Pantelides, C. P., Gibbons, M. E., and Reaveley, L. D. (2013). "Axial Load Behavior of concrete columns confined with GFRP spirals." *Journal of composites for construction* May/June 2013, 305-313.

Tobbi, H., Farghaly, A.S., and Benmokrane, B. (2012). "Concrete columns reinforced longitudinally and transversely with glass fibre-reinforced polymer bars." *ACI Struct. J.,* 109(4), 551-558.

Tan, K. H (2003). "Fibre-reinforced polymer reinforced for concrete structures." FRPRCS-6 2003 Singapore.